Cell Reports

Resource

Phosphoproteomic responses of TORC1 target kinases reveal discrete and convergent mechanisms that orchestrate the quiescence program in yeast

Graphical abstract

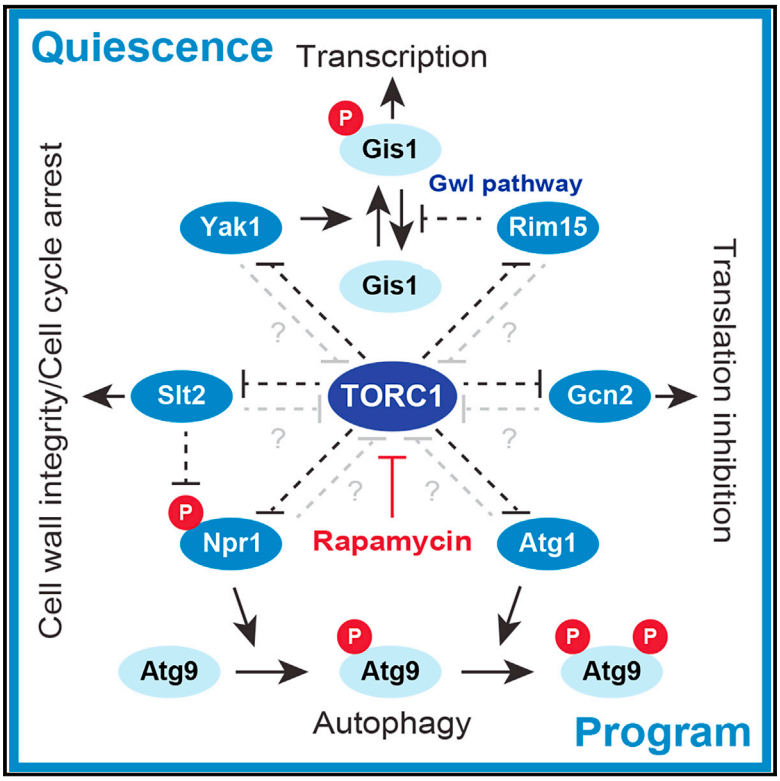

Highlights

- TORC1 effector kinases orchestrate the rapamycin-sensitive phosphoproteome
- Npr1, Rim15, Slt2, and Yak1 engage in TORC1 feedback control circuits
- Yak1 and $PP2A^{Cdc55}$ delineate a functionally coupled kinase-phosphatase module
- Npr1 controls the rate of autophagosome assembly via Atg9

Authors

Ladislav Dokládal, Michael Stumpe, Zehan Hu, Malika Jaquenoud, Jörn Dengjel, Claudio De Virgilio

Correspondence

joern.dengjel@unifr.ch (J.D.), claudio.devirgilio@unifr.ch (C.D.V.)

In brief

The molecular pathways linking TORC1 to distal readouts defining the quiescence program involve the Atg1, Gcn2, Slt2/Mpk1, Npr1, Rim15, and Yak1 kinases. Here, Dokládal et al. use *in vivo* quantitative phosphoproteomics to elucidate the architecture of the respective kinase network that involves discrete, convergent, and multilayered feedback regulatory mechanisms.

Dokládal et al., 2021, Cell Reports *37*, 110149
December 28, 2021
https://doi.org/10.1016/j.celrep.2021.110149

CellPress

Cell Reports

CellPress
OPEN ACCESS

Resource

Phosphoproteomic responses of TORC1 target kinases reveal discrete and convergent mechanisms that orchestrate the quiescence program in yeast

Ladislav Dokládal,[1,2] Michael Stumpe,[1,2] Zehan Hu,[1] Malika Jaquenoud,[1] Jörn Dengjel,[1,*] and Claudio De Virgilio[1,3,*]
[1]Department of Biology, University of Fribourg, 1700 Fribourg, Switzerland
[2]These authors contributed equally
[3]Lead contact
*Correspondence: joern.dengjel@unifr.ch (J.D.), claudio.devirgilio@unifr.ch (C.D.V.)
https://doi.org/10.1016/j.celrep.2021.110149

SUMMARY

The eukaryotic TORC1 kinase assimilates diverse environmental cues, including growth factors and nutrients, to control growth by tuning anabolic and catabolic processes. In yeast, TORC1 stimulates protein synthesis in response to abundant nutrients primarily through its proximal effector kinase Sch9. Conversely, TORC1 inhibition following nutrient limitation unlocks various distally controlled kinases (e.g., Atg1, Gcn2, Npr1, Rim15, Slt2/Mpk1, and Yak1), which cooperate through poorly defined circuits to orchestrate the quiescence program. To better define the signaling landscape of the latter kinases, we use *in vivo* quantitative phosphoproteomics. Through pinpointing known and uncharted Npr1, Rim15, Slt2/Mpk1, and Yak1 effectors, our study examines the architecture of the distally controlled TORC1 kinase network. Accordingly, this is built on a combination of discrete, convergent, and multilayered feedback regulatory mechanisms, which likely ensure homeostatic control of and/or robust responses by TORC1 and its effector kinases under fluctuating nutritional conditions.

INTRODUCTION

The target of the rapamycin complex 1 (TORC1) pathway pivotally regulates eukaryotic cell growth and couples diverse environmental signals, including growth factors, hormones, and nutrients, to downstream effectors to control anabolic (e.g., protein translation) and catabolic (e.g., macroautophagy) processes in a reciprocal manner (González and Hall, 2017; Sarbassov et al., 2005). Deregulation of mammalian TORC1 (mTORC1) in humans is associated with pathologies including cancer, obesity, type 2 diabetes, and neurodegeneration (Cornu et al., 2013; Liu and Sabatini, 2020), which emphasizes its central role in growth control. In yeast, nutrient-rich media stimulate TORC1, which subsequently promotes mRNA translation and ribosome biogenesis (Ribi) by directly phosphorylating effectors, such as the protein kinase Sch9 and the transcriptional regulator Sfp1 (Huber et al., 2009, 2011; Jorgensen et al., 2004; Lee et al., 2009; Lempiäinen et al., 2009; Urban et al., 2007). Conversely, nutrient limitation or rapamycin treatment attenuate signaling through TORC1, which drives cells into a quiescent state that is characterized by a distinct array of physiological, biochemical, and morphological traits (De Virgilio, 2012; Zaragoza et al., 1998). The molecular pathways that link TORC1 to these distal readouts involve several protein kinases, including Atg1, Gcn2, Slt2/Mpk1, Npr1, Rim15, and Yak1, which cooperatively orchestrate the quiescence program (Figure 1).

Reduced TORC1-mediated phosphorylation of Atg13, for instance, allows it to form a complex with and thereby activate Atg1, which then initiates macroautophagy to recycle macromolecular complexes and cellular components via autophagosome-mediated vacuolar/lysosomal degradation (Kamada et al., 2010; Mizushima et al., 2011). In parallel, inactivation of TORC1 also reduces the phosphorylation state of Tap42, a regulator of type 2A and type 2A-like (e.g., Sit4) protein phosphatases (PP2A) (Di Como and Arndt, 1996; Jiang and Broach, 1999), which triggers the dephosphorylation of residues in and activates Gcn2 and Npr1. The respective Sit4-dependent dephosphorylation of serine 577 (Ser^{577}) in Gcn2 enhances its affinity for uncharged tRNAs and thus stimulates its kinase activity toward the α-subunit of eIF2 (eIF2α) to inhibit general translation initiation (Cherkasova and Hinnebusch, 2003; Hinnebusch, 2005). Similarly, reduced TORC1 levels favor Sit4-mediated dephosphorylation and activation of Npr1 (Gander et al., 2008; Jacinto et al., 2001; Schmidt et al., 1998), which regulates the sorting, stability, and/or activity of nutrient permeases at the plasma membrane (Boeckstaens et al., 2014, 2015; De Craene et al., 2001; MacGurn et al., 2011; Merhi and André, 2012).

The mechanisms that release Rim15 from TORC1 inhibition have also been elucidated in considerable detail. Accordingly, Sch9 inactivation and likely activation of PP2A and/or Sit4 combined result in dephosphorylation of 14-3-3 protein binding sites within Rim15, which allows it to dissociate from the cytoplasmic anchor proteins Bmh1/2 and enter the nucleus (Pedruzzi et al., 2003; Wanke et al., 2005, 2008). Activation of Rim15 kinase activity, however, additionally requires inactivation of protein kinase A (PKA) (Reinders et al., 1998), which is triggered by TORC1 inactivation via a circuit that involves the stimulation of

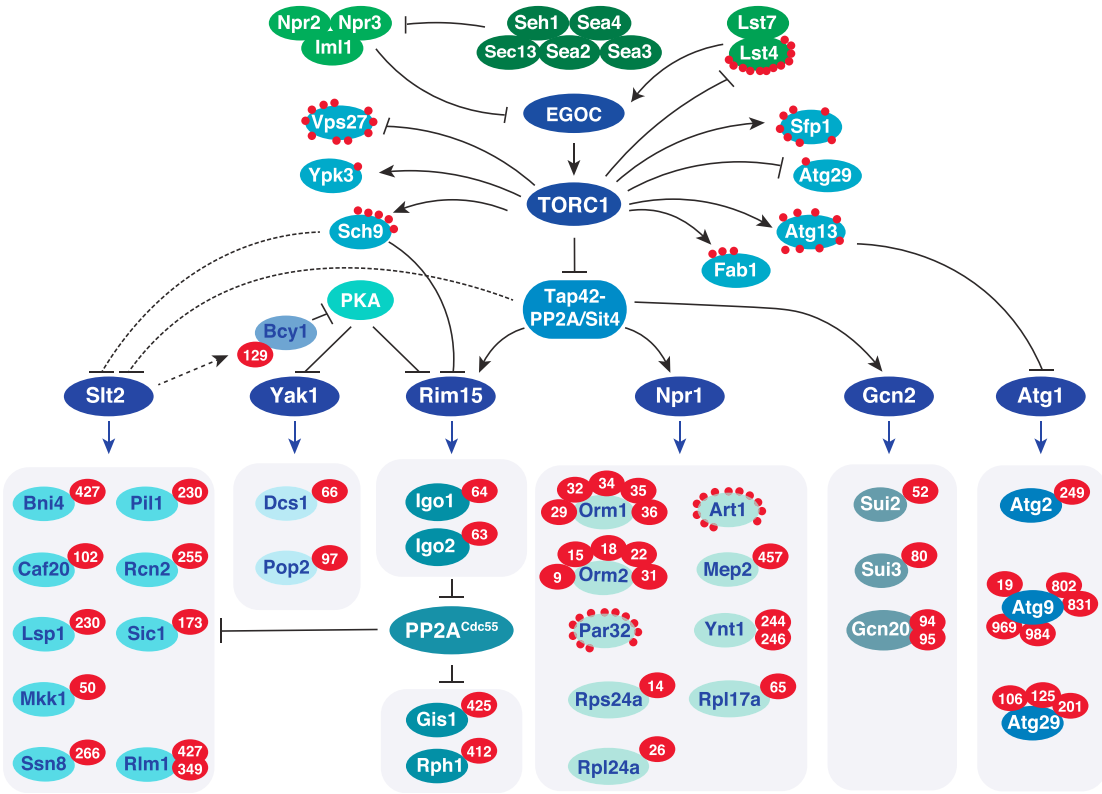

Figure 1. The TORC1 signaling network in budding yeast

The heterodimeric Rag GTPases Gtr1-Gtr2 control TORC1 as part of the vacuolar membrane-associated pentameric EGO (exit from rapamycin-induced growth arrest) complex (EGOC). Their TORC1-stimulating state (i.e., $Gtr1^{GTP}$-$Gtr2^{GDP}$) is controlled by the heterotrimeric SEA-subcomplex that inhibits TORC1 (SEACIT; containing Npr2, Npr3, and Iml1) and the heterodimeric Lst4-Lst7 GAP (GTPase-activating) complex, which respond to amino acids through poorly understood mechanisms. The SEA (Seh1-associated) subcomplex that activates TORC1 (SEACAT) contains Seh1, Sea2–4, and Sec13 and antagonizes the GAP function of SEACIT (Powis and De Virgilio, 2016). TORC1 favors growth-stimulating, anabolic processes such as mRNA translation and Ribi and inhibits catabolic processes (e.g., macroautophagy) and stress responses through direct control of proximal targets that include the protein kinases Sch9 and Ypk3, the transcriptional regulator Sfp1, Atg29 and the regulatory subunit of the Atg1 signaling complex Atg13, Vps27, a subunit of the heterodimeric endosomal sorting complex required for transport (ESCRT-0), and the phosphatidylinositol-3-phosphate 5-kinase Fab1 (Chen et al., 2021; González et al., 2015; Hatakeyama et al., 2019; Hu et al., 2019; Klionsky et al., 2021; Lempiäinen et al., 2009; Loewith and Hall, 2011; Urban et al., 2007; Yerlikaya et al., 2016). The Tap42-PP2A/Sit4 protein phosphatase complexes also constitute a key effector branch of TORC1, although it remains mechanistically unclear whether TORC1 controls these modules via phosphorylation of Tap42 or the Tap42-interactor Tip41 (Jacinto et al., 2001; Jiang and Broach, 1999). TORC1 also directly phosphorylates Lst4 as part of a negative feedback control mechanism (Péli-Gulli et al., 2017). The distally controlled protein kinases that orchestrate the quiescence program upon TORC1 downregulation include Atg1, Gcn2, Npr1, Slt2, Rim15, and Yak1. Red circles containing a number denote experimentally studied residues in proteins that are directly phosphorylated by one of these six protein kinases, except for the ones in Gis1 and Rph1, which are phosphorylated by an unknown protein kinase but dephosphorylated via the Rim15-Igo1/2-$PP2A^{Cdc55}$ Gwl pathway (see Tables S1 and S2). Arrows and bars denote positive and negative interactions, respectively. Solid arrows and bars refer to direct interactions; dashed bars refer to indirect and/or potential interactions. Blue arrows (downstream of Atg1, Gcn2, Npr1, Slt2, Rim15, and Yak1) indicate activating or inhibitory phosphorylation events. Red circles without numbers denote amino acid residues that are directly phosphorylated by TORC1. For further details, see text.

the mitogen-activated protein kinase (MAPK) Slt2 (downstream of Sch9 and likely Sit4) and Slt2-mediated phosphorylation and activation of the inhibitory PKA subunit Bcy1 (Krause and Gray, 2002; Kuranda et al., 2006; Soulard et al., 2010; Torres et al., 2002) (Figure 1). Of note, Slt2 is also the most distal effector of a serially wired protein kinase cascade (i.e., Pkc1, Bck1, Mkk1/2, and Slt2), coined the cell wall integrity (CWI) pathway, that remodels the cell wall in response to a variety of stresses including nutrient limitation (Jiménez-Gutiérrez et al., 2020; Levin, 2005), which also explains its importance for the survival of quiescent cells (Ai et al., 2002; Krause and Gray, 2002). Interestingly, like the orthologous greatwall kinase (Gwl) in higher eukaryotes, active Rim15 phosphorylates a conserved residue within endosulfines (i.e., the paralogous Igo1/2 proteins in yeast), thereby converting them to inhibitors of the Cdc55-protein phosphatase 2A ($PP2A^{Cdc55}$ or PP2A-B55δ in higher eukaryotes) (Bontron et al., 2013; Gharbi-Ayachi et al., 2010; Mochida et al., 2010). This inhibition of $PP2A^{Cdc55}$ contributes to the induction of the gene expression program in quiescent cells by preventing both the dephosphorylation and consequently inactivation of the transcriptional activator Gis1 and the activation of the paralogous transcriptional repressor Rph1 (Bernard et al., 2015; Bontron et al., 2013; Pedruzzi et al., 2000). In addition, $PP2A^{Cdc55}$ inhibition also promotes G_1 cell cycle arrest as this enables the B-type cyclin (Clb) cyclin-dependent protein kinase (CDK) inhibitor Sic1 to preserve its Slt2-mediated phosphorylation (at Ser^{173}) and thereby

escape degradation by the proteasome (Moreno-Torres et al., 2015, 2017) (Figure 1).

In parallel to controlling Rim15 activity, PKA also inhibits the nuclear localization and activation of the dual-specificity tyrosine-regulated protein kinase (DYRK) Yak1 through direct phosphorylation, which tethers inactive Yak1 to the cytoplasmic 14-3-3 anchor proteins Bmh1/2 (Garrett et al., 1991; Lee et al., 2011; Malcher et al., 2011; Schmelzle et al., 2004). Inactivation of TORC1 therefore also results, via the Sch9 –| Slt2 → Bcy1 –| PKA branch, in nuclear translocation and activation of Yak1, which (directly or indirectly) targets several transcription factors to control stress response and ribosomal protein gene expression and thereby contributes to the stress resistance and chronological lifespan of quiescent cells (Cao et al., 2016; Lee et al., 2008; Malcher et al., 2011; Martin et al., 2004).

While our current knowledge indicates that TORC1 controls the establishment of a quiescent state largely via its distal effectors Atg1, Gcn2, Slt2, Npr1, Rim15, and Yak1, as outlined above, we still know comparably little on whether each of these protein kinases executes primarily a separate set of individual tasks, whether they act to some extent redundantly or share common functions, and whether they are embedded in more complex networks involving cross-communications and regulatory feedback loops to ensure robust and homeostatic cellular responses. To begin to address these outstanding questions, we set out to establish the Slt2-, Rim15-, Npr1-, and Yak1-dependent *in vivo* phosphoproteomes in rapamycin-treated cells and combined these data with our recently published Atg1- and Gcn2-dependent phosphoproteome data that were carried out under the same conditions (Dokládal et al., 2021; Hu et al., 2019). Accordingly, we present here a compendium of *in vivo* phosphorylation events that are partitioned between these six TORC1-controlled protein kinases. Our data confirm the expectation that Gcn2 and Atg1 show target profiles that are primarily dedicated to the control of protein synthesis and macroautophagy, respectively. Intriguingly, however, they also reveal that Yak1 and the Rim15-Igo1/2-PP2A^{Cdc55} Gwl pathway converge on a large set of common residues within various proteins, indicating that the Yak1-PP2A^{Cdc55} kinase-phosphatase pair coevolved to coordinately control the phosphorylation state of shared residues, as we also illustrate with a functional study of such residues in Gis1. Finally, our combined results also indicate that Slt2 likely acts upstream of Npr1 to control specific effectors, that Npr1 plays a role in the regulation of macroautophagy, and that Atg1, Gcn2, Slt2, Npr1, Rim15, and Yak1 are wired to each other through multilayered feedback regulatory loops that likely ensure homeostatic control of and/or robust responses by TORC1 under fluctuating nutritional conditions.

RESULTS AND DISCUSSION

The rapamycin-sensitive phosphoproteome: Distal effector kinases orchestrate the quiescence program

To cover comprehensively phosphorylation-based signaling events of the distally controlled TORC1 target kinases Atg1, Gcn2, Npr1, Rim15, Slt2, and Yak1, we followed a two-tiered strategy: we used our recently published Atg1- and Gcn2-dependent phosphoproteomes (Dokládal et al., 2021; Hu et al., 2019) and performed a set of 18 stable isotope labeling by amino acids in cell culture (SILAC)-based quantitative phosphoproteomic experiments comparing wild-type with *npr1Δ*, *rim15Δ*, *slt2Δ*, and *yak1Δ* cells (Figure 2A). Cells were left untreated or treated with the allosteric TORC1 inhibitor rapamycin for 30 min to ensure that the kinases of interest (KoI; i.e., Slt2, Npr1, Rim15, and Yak1) were robustly activated in wild-type cells. Differentially labeled cells were mixed and processed for liquid chromatography-tandem mass spectrometry (LC-MS)/mass spectrometry (MS)-based phosphoproteomic analyses as outlined in Figure 2A (see STAR Methods for details). For each protein kinase mutant, we recorded three biological replicates comparing (1) wild-type and *KoIΔ* cells both treated with rapamycin and (2) rapamycin-treated and untreated *KoIΔ* cells as negative control. In total, we identified more than 48,000 phosphosites on 4,846 proteins (Figure 2B). In combination with our published data (Dokládal et al., 2021; Hu et al., 2019), we analyzed 37 phosphoproteomic experiments, which is, to our knowledge, currently the largest dataset addressing rapamycin-sensitive phosphosites in yeast. Based on these data, we estimate that our experimental setup allows the identification of up to maximally 50,000 phosphorylation sites, which indicates that our data cover more than 96% of the experimentally detectable yeast phosphoproteome under the conditions tested (Figure 2C). In general terms, we further deduced from these results that yeast proteins carry on average five phosphorylated residues spaced, again on average, by 64 amino acids (Figures 2D and 2E), which matches reasonably well with the estimated mean length of 415 amino acids for yeast proteins (Drummond et al., 2005). Interestingly, highly phosphorylated proteins (containing more than 45 phosphosites) appear to be primarily associated with nuclear pores, bud necks, and mating projections (Figure 2F). Conversely, non-phosphorylated proteins localized mainly to the endoplasmic reticulum (ER) and mitochondria (Figure 2G), which may be explained by the low number of protein kinases associated with these organelles, while the underrepresentation of non-phosphorylated proteins associated with chromatin may be linked to the electrostatic interference of phosphorylated residues with chromatin (Li et al., 2021).

Of the 48,058 identified sites, we were able to quantify 43,686 (Figure 2B). We then removed those sites that could not be clearly localized to a specific amino acid residue (probability > 0.75, class I sites according to Olsen et al., 2006) and normalized the remaining sites to protein levels to discriminate regulated phosphosites from regulated proteins. For each KoI, we requested a minimum of three datapoints of biological replica, of which minimally one had to derive from the comparison of rapamycin-treated wild-type and *KoIΔ* cells. This led to an average of more than 18,500 phosphosites per KoI (Figure 2B; Table S1). Among these sites, we screened for potential KoI target sites, applying the following criteria: sites had to be significantly positively regulated and exhibit a minimum 2-fold change comparing (1) rapamycin-treated and untreated wild-type cells and (2) rapamycin-treated wild-type and *KoIΔ* cells (random effect model, 95% confidence interval; Hu et al., 2019). In addition, phosphosites that were regulated when comparing rapamycin-treated and untreated *KoIΔ* cells (negative control) were removed from the final shortlist, which contained 120, 19, 167, 89, 29, and 73 potential Atg1, Gcn2, Npr1, Rim15, Slt2, and Yak1 target residues that fulfilled

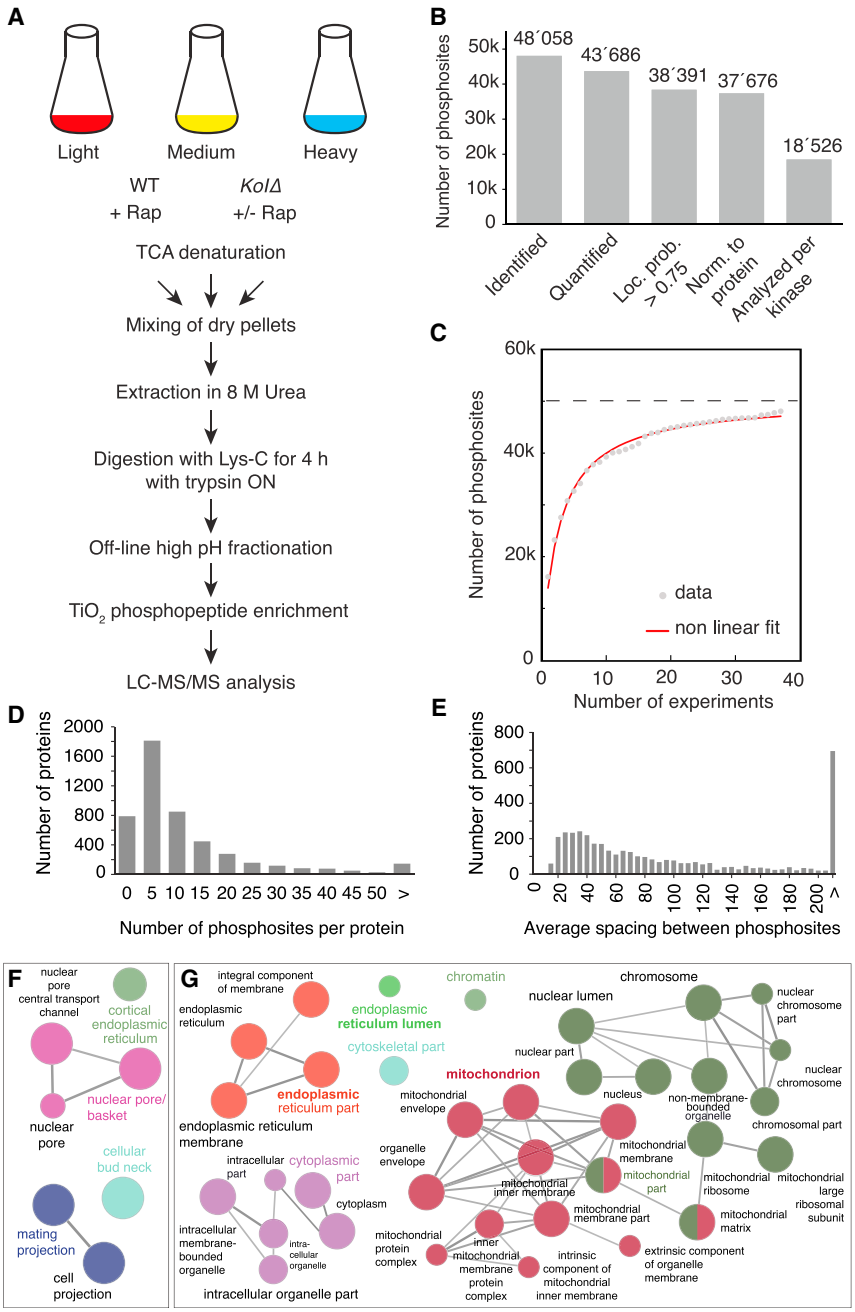

Figure 2. Quantitative phosphoproteomics of rapamycin-treated yeast protein kinase mutants

(A) Quantitative MS-based proteomics workflow. Yeast cells were labeled by Lys0, Arg0 (light); Lys4, Arg6 (medium); or Lys8, Arg10 (heavy) amino acid variants and samples processed as outlined.

(B) Identified phosphosites. Data filtering steps are indicated.

(C) Cumulatively identified phosphosites. In 37 SILAC experiments, a total of 48,058 phosphosites were identified. A non-linear fit (red line) of datapoints (gray circles) indicates saturation and predicts a total of 50,417 identifiable phosphosites (black dashed line).

(D) Number of phosphosites per protein. Phosphosite numbers are binned according to x axis labels, and respective protein counts are indicated on the y axis.

(E) Average spacing between phosphosites within proteins. Average spacings between phosphosites (in number of amino acids) are binned according to x axis labels, and respective protein counts are indicated on the y axis.

(F and G) GO analysis of proteins carrying more than 45 (F) or no (G) phosphosites. Listed are significantly enriched GO terms ($p < 0.05$, Bonferroni step-down corrected). Sizes of nodes represent significance. Coloring indicates GO term grouping based on shared genes between respective terms. The leading group term is based on highest significance. Common groups between (F) and (G) were removed. See also Table S1.

all of our high-stringency criteria (Table S2). In the following paragraphs, we will briefly discuss our data on Npr1, Rim15, Slt2, and Yak1 in the context of the current literature.

Npr1-dependent phosphoproteome analyses have so far been carried out with both exponentially growing and rapamycin-treated cells (Li et al., 2019; MacGurn et al., 2011). In the former study, loss of Npr1 was associated with a weak phosphoproteomic response, which is not surprising because Npr1 is predominantly inactive in exponentially growing cells (Li et al., 2019). In the latter study with rapamycin-treated cells, however, loss of Npr1 seemingly caused a significant phosphoproteomic response, although the extent of this response remained largely elusive as the primary mass spectrometry data remained undisclosed (MacGurn et al., 2011). Here, we not only recovered and provided the target residues for most Npr1 effector proteins identified in the latter study but also (1) detected the majority of the currently known Npr1 target residues in various proteins (e.g., in Art1/Ldb19, Orm2, Mep2, and Par32 [Boeckstaens et al., 2014; Boeckstaens et al., 2015; Breslow et al., 2010; MacGurn et al., 2011; Shimobayashi et al., 2013; Varlakhanova et al., 2018]), (2) identified residues in potential Npr1 targets (e.g., Rho5, Bul1/2, and Pib2 [Annan et al., 2008; Brito et al., 2019; Merhi and André, 2012]), and (3) pinpointed 86 uncharted Npr1 targets (Figure 3; Table S2). Together with our deduced kinase consensus motif for Npr1 (Figure 3), our Npr1-directed phosphoproteome therefore provides a wealth of interesting leads for future studies.

The study by Li and co-workers also included *rim15*Δ cells, which only weakly affected the phosphoproteome in exponentially growing cells (Li et al., 2019). Nevertheless, this study was able to identify the only currently known *bona fide* target

CellPress
OPEN ACCESS

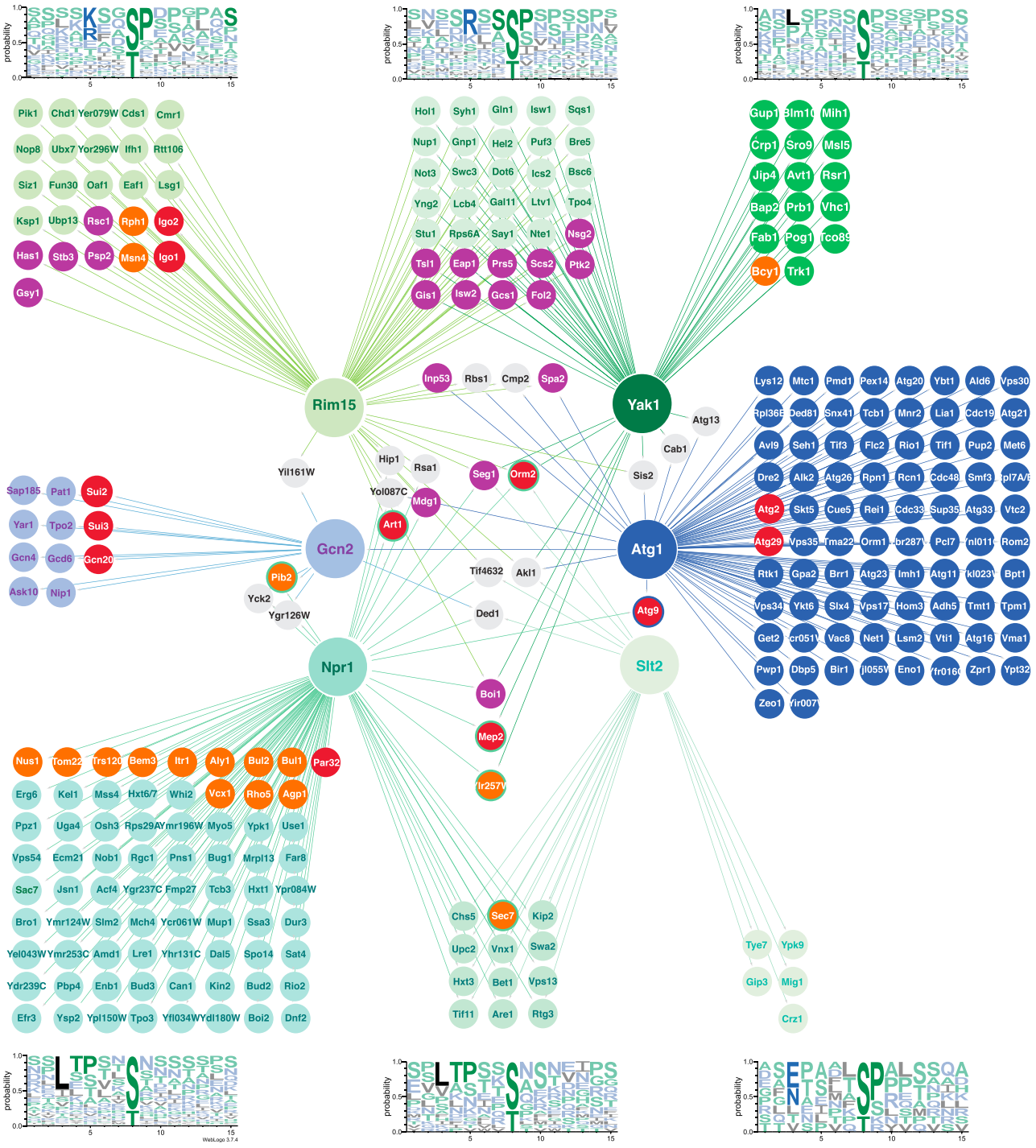

Figure 3. Target interaction network of Atg1, Gcn2, Npr1, Rim15, Slt2, and Yak1

Potential target proteins (containing at least one protein kinase target residue) were extracted from Table S1 and visualized with Cytoscape 3.8.2 (Shannon et al., 2003). Motif analyses were generated based on all regulated phospho-residues within the associated clusters of proteins using WebLogo (Crooks et al., 2004). Red circles denote proteins with experimentally confirmed protein kinase target residues. Orange circles denote proteins with potential protein kinase target residues, which were identified by phosphoproteomic, gel electrophoretic mobility, or protein kinase assays (Table S2). Purple circles denote Rim15-regulated proteins for which we recovered at least one Rim15-controlled phospho-peptide, which, based on published proteomics analyses, has previously been found to be regulated by $PP2A^{Cdc55}$ (Table S2). Art1, Orm2, Mep2, Pib2, Ylr257W, and Sec7 contain confirmed or potential Npr1 target residues, but may also be regulated by at least one other kinase. Similarly, Atg9 contains known Atg1 target residues (Figure 1) but may also be phosphorylated by Npr1 at Ser^{122} (Table S1). See also Figures S1–S5 and Tables S2 and S3.

residues of Rim15 (i.e., Ser^{64} and Ser^{63} in the PP2A^{Cdc55} inhibitors Igo1 and Igo2, respectively) as top hits, which fits well with the reported role of Rim15 in coordinating the G_1-S transition in response to both cell cycle cues that emanate from the cyclin-dependent protein kinase Cdc28 in exponentially growing cells and nutrient signals that are mediated by TORC1 (Moreno-Torres et al., 2017). In our current study, we recovered 89 potential Rim15 target residues, including Igo1-Ser^{64} and Igo2-Ser^{63} (but did not detect any Rim15-regulated residues in the poorly expressed transcription factors Hsf1 and Msn2 that can be phosphorylated *in vitro* by Rim15 [Lee et al., 2013]). Importantly, because the combined loss of Igo1 and Igo2 virtually phenocopies the loss of Rim15 (Talarek et al., 2010), we expected our Rim15-regulated phosphoproteome to mainly cover residues that are directly regulated by PP2A^{Cdc55} rather than by Rim15. In support of this assumption, we found the consensus motif for *in vivo* Rim15-regulated sites (Figure 3) to perfectly match the proposed PP2A^{Cdc55}-directed (S/T)P motif (Baro et al., 2018; Godfrey et al., 2017; Mok et al., 2010). Moreover, and even more strikingly, 32.5% of our Rim15-regulated residues have independently been identified as potential PP2A^{Cdc55} targets (Baro et al., 2018; Touati et al., 2019) (Table S2). Thus, Rim15 appears to primarily impinge on phospho-residues via PP2A^{Cdc55}, and our respective phosphoproteome, while exquisitely well-covering earlier work, also singled out 56 additional potential effectors of the Gwl pathway. Among these, we would like to specifically highlight the transcriptional repressor Rph1 that is known to inhibit autophagy downstream of Rim15 and in which we identified Ser^{412} as a Rim15-regulated residue (Bernard et al., 2015). In addition, Rim15 also controls the phosphorylation state of residues in the glycogen synthase Gsy1 and the large subunit of trehalose 6-phosphate synthase/phosphatase complex Tsl1, which may explain why *rim15*Δ mutants are unable to accumulate these reserve carbohydrates upon entry into quiescence (Cao et al., 2016; Reinders et al., 1998).

An Slt2-dependent phosphoproteome analysis has so far been carried out with exponentially growing cells, where Slt2 is predominantly inactive (Li et al., 2019). A comparison of our rapamycin-sensitive, Slt2-dependent phosphoproteome with the latter study therefore expectedly revealed little target overlap. Here, we found that Slt2 potentially targets 29 residues, of which seven (in five proteins) seemed to be exclusively regulated by Slt2, while the majority of the other residues were also co-regulated by Npr1 (see below). This small cluster of Slt2-specific target residues, which defined a proline-directed (S/TP) kinase motif that is characteristic for MAPKs (Figure 3) (Übersax and Ferrell, 2007), pinpoints a role for Slt2 in controlling the calcineurin-activated transcription factor Crz1 and the transcriptional repressor Mig1 (Figure 3 and Table S2). Because Crz1 has previously been reported to cooperate with the CWI pathway in cell wall remodeling and Mig1 presumably mediates glucose repression downstream of Pkc1 (Mishra et al., 2017; Salgado et al., 2002), these findings warrant future mechanistically oriented studies of the respective phosphorylation events. Curiously, our Slt2 target profile did not include a number of proteins and residues that are otherwise known to be phosphorylated by Slt2 under a variety of stress conditions (Table S2). While this may be explained in part by the fact that phosphopeptides can escape detection by mass spectrometry because of their low abundance (e.g., Bcy1 and Sic1), their physical properties, and/or experimental differences in phosphopeptide purification protocols, we also deem it possible that TORC1 inactivation and different stresses could each prime and direct Slt2 toward specific subsets of effectors. Such a model would also be in line with the observation that different stresses, such as mechanical, oxidative, hypo-osmotic, or heat stress, laterally impinge on individual elements of the CWI pathway (Harrison et al., 2004).

Finally, to our knowledge, previous phosphoproteome studies have so far not included *yak1*Δ cells. With respect to the Yak1 target proteins proposed in the literature, our rapamycin-sensitive phosphoproteome of *yak1*Δ cells identified residues in Bcy1 (Griffioen et al., 2001) but was unable to capture any residues in the poorly expressed transcription factors Hsf1, Msn2, Ifh1, and Crf1, or in the mRNA-modifying enzymes Dcs1 and Pop2 (Kim et al., 2011; Lee et al., 2008; Malys et al., 2004; Martin et al., 2004; Moriya et al., 2001). Notably, however, our list of 60 potential Yak1 target proteins is likely to contain numerous biologically relevant hits (Figure 3), because we found, surprisingly, that a large fraction of the Yak1-controlled residues are simultaneously targeted by the Gwl pathway (see below).

Atg1 and Gcn2 implement discrete facets of the quiescence program

For a global overview on how Atg1, Gcn2, Npr1, Slt2, Rim15, and Yak1 partition the regulation of their downstream effectors, we next performed Gene Ontology (GO) term enrichment analyses of all proteins carrying significantly regulated phosphosites (Table S2). As previously published, Gcn2 and Atg1 have target profiles that are dedicated mainly to the control of protein synthesis and autophagy, respectively (Dokládal et al., 2021; Hu et al., 2019), and these profiles overlap only marginally with the ones of Npr1, Slt2, Rim15, and Yak1 as visualized by our detailed protein target interaction network (Figures 3 and S1). Interestingly, however, Atg1 controls the phosphorylation state of Ser^{136} at the end of the Gcn1-binding domain in Gcn2 (Hinnebusch, 2005) (Figure 3; Table S2), pinpointing the existence of a potentially intriguing direct crosstalk between these kinases.

PP2A^{Cdc55} and Yak1 delineate a functionally coupled phosphatase-kinase module

Like Atg1 and Gcn2, Rim15 and Yak1 each regulate their own specific subsets of cellular events but also clearly co-regulate various processes such as chromatin remodeling, lipid biosynthesis, and mRNA catabolism (Figure S1). Strikingly, Rim15 and Yak1 potentially control the latter processes through a significant proportion of shared target proteins (>51% for each kinase), with a majority (>75%) of regulated amino acid residues in these proteins being (directly or indirectly) targeted by both kinases (Figure 3; Table S2). These data can most easily be explained with a model in which Rim15 controls Yak1 target residues via Igo1/2-mediated inhibition of PP2A^{Cdc55}, which is not only supported by previous observations that placed Rim15 and Yak1 parallel to each other in the control of chronological lifespan-promoting transcriptional events (Cao et al., 2016; Zhang et al., 2013), but also by the similarity of our Yak1- and PP2A^{Cdc55}-directed sequence motifs (Figure 3). To experimentally address this

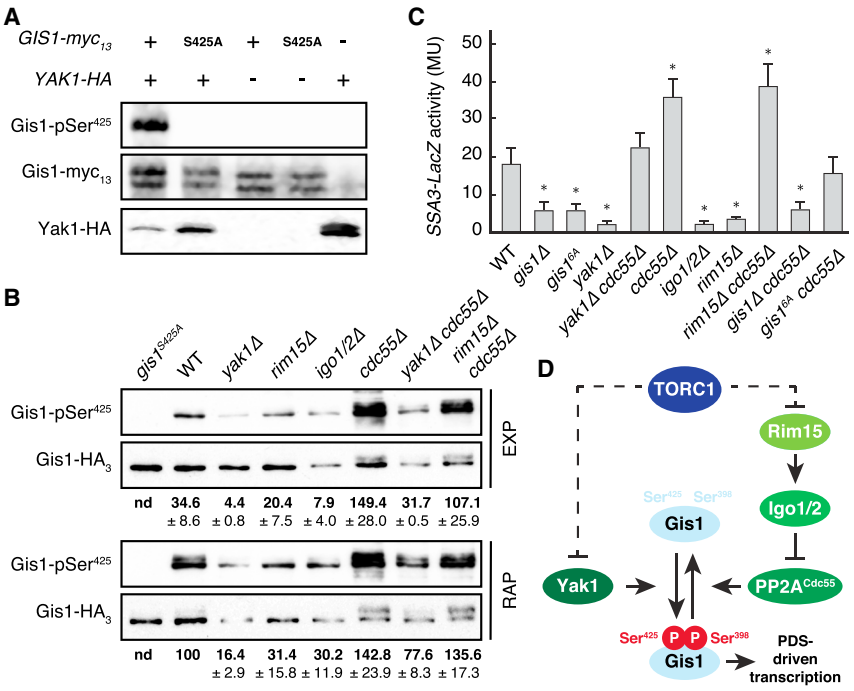

Figure 4. The Gwl pathway and Yak1 converge on Gis1-Ser$^{398/425}$

(A) Phosphorylation of Gis1-Ser^{425} in recombinant bacteria. Recombinant Gis1-myc$_{13}$ variants were co-expressed, or not, with recombinant Yak1-HA. Bacterial lysates were then analyzed by immunoblotting using anti-pSer^{425}-Gis1, anti-c-Myc, and anti-HA antibodies.

(B) Phosphorylation of Gis1-Ser^{425} or Gis1-HA$_3$ in exponentially growing (EXP) and rapamycin-treated (RAP; 200 ng ml^{-1}, 30 min) wild-type (WT) and indicated mutant yeast strains expressing plasmid-encoded Gis1-HA$_3$. Whole cell lysates were analyzed as in (A). The mean ratios of Gis1-pS^{425}/Gis1-HA$_3$ (n = 3; ±SD) were normalized to the one of rapamycin-treated WT cells (set to 100%).

(C) *SSA3-LacZ* expression (in Miller units) in glucose-limited, post-diauxic WT and indicated mutant strains (n = 3; +SD; data are presented as means). Unpaired Student's t tests were used to determine significant differences when compared to the respective WT control (*p ≤ 0.05; **p ≤ 0.001; ***p ≤ 0.0001).

(D) Model for the control of Gis1 by the Yak1-PP2A^{Cdc55} protein kinase-phosphatase module. Arrows and bars denote positive and negative interactions, respectively. Solid arrows and bars refer to direct interactions; dashed bars refer to indirect interactions. For details see text.

intriguing model, we decided to study whether Rim15 and Yak1 may, as predicted by our phosphoproteome data, separately impinge on the transcription factor Gis1. Notably, PP2A^{Cdc55} is known to dephosphorylate Ser^{425} in Gis1 and thereby inhibit its recruitment to the promoter regions of post-diauxic shift element (PDS)-controlled genes (Bontron et al., 2013; Pedruzzi et al., 2000). Inactivation of TORC1 (following rapamycin treatment or glucose limitation) and consequent stimulation of the Gwl pathway therefore activates Gis1-driven, PDS-element-dependent transcription, which is in part due to PP2A^{Cdc55} inhibition and activation of a protein kinase that ensures Ser^{425} phosphorylation and hence promoter recruitment of Gis1. In this context, our phosphoproteome data indicated that Yak1 impinges on Ser^{398} (Table S2) and, applying less stringent selection criteria (Table S1), also on Ser^{425} in Gis1. To test whether Yak1 directly phosphorylates Gis1-Ser^{425}, we then assayed Yak1 kinase activity *in vivo* by co-expressing Yak1 and Gis1 in bacteria. Using phosphospecific anti-Gis1-pSer^{425} antibodies, we found that Yak1 indeed phosphorylated Ser^{425} in Gis1 when Yak1 was co-expressed with Gis1, but not when it was co-expressed with Gis1^{S425A} or when Yak1 and Gis1 were expressed individually (Figure 4A). In addition, loss of Yak1, like loss of Rim15 or loss of Igo1/2, strongly reduced the steady-state levels of Gis1-pSer^{425} in exponentially growing yeast cells and largely prevented the rapamycin-induced increase in Gis1-Ser^{425} phosphorylation observed in wild-type cells (Figure 4B). Conversely, loss of Cdc55 significantly boosted Gis1-Ser^{425} phosphorylation in exponentially growing and, even more robustly, in rapamycin-treated cells in a strongly Yak1-dependent, but Rim15-independent manner. Thus, the phosphorylation state of Gis1-Ser^{425} is primarily defined by the Yak1-PP2A^{Cdc55} protein kinase-phosphatase pair, although an additional protein kinase may ensure the residual phosphorylation of Gis1-Ser^{425} that we observed in rapamycin-treated *yak1*Δ cells. Yak1, like Rim15, has previously been shown to be required for Gis1-dependent transcription of *SSA3* in rapamycin-treated cells (Zhang et al., 2013), which is mediated by three PDS elements in the promoter of *SSA3* (Boorstein and Craig, 1990; Pedruzzi et al., 2000). Here, we found that loss of Yak1, like loss of Gis1, Rim15, or Igo1/2 combined, and similar to the expression of a Gis1 allele with Ser to alanine (Ala) replacements of the 6 Ser residues surrounding and including Ser^{398} and Ser^{425} (Gis1^{6A}), strongly reduced *SSA3-lacZ* expression in glucose-limited cells (Figure 4C). Loss of Cdc55, however, hyperactivated *SSA3-lacZ* expression under the same conditions, and this effect was fully abrogated by loss of Gis1, but not by loss of Rim15, and significantly and similarly reduced by loss of Yak1 or the expression of the Gis1^{6A} allele. Thus, our data corroborate our assumption that Yak1 and the Gwl pathway coordinately control and converge on Ser$^{398/425}$ of Gis1 (Figure 4D) but also indicate that PP2A^{Cdc55} regulates Gis1 function in part via a Ser$^{398/425}$- and Yak1-independent mechanism, which is in line with previous conclusions (Bontron et al., 2013). In sum, our Gis1-centered experiments provide a proof of principle for a more general model put forward by our phosphoproteome data, namely that Yak1 and the Gwl pathway have coevolved to coordinately control the phosphorylation state of common target residues. Such a design principle, i.e., the functional coupling of a kinase and phosphatase, is not without precedent (e.g., the Ca^{2+}/calmodulin-regulated phosphatase calcineurin has also co-evolved with specific protein kinases to jointly control shared effectors), favors robust cellular responses, and endorses the evolutionary acquisition of additional downstream targets while preserving network architecture and wiring of feedforward regulatory loops (Goldman et al., 2014).

Slt2 modulates Npr1 function

Interestingly, 72% (16/22) of the Slt2-regulated proteins were also regulated by Npr1, and all but one (Orm2-Ser^{18}) of 29 residues in the respective proteins were coregulated by Slt2 and Npr1 (Table S2; Figure 3). Because the consensus phosphorylation motif of the latter cohort almost perfectly matched the Npr1-specific, but not the proline-directed, Slt2 motif, we considered the possibility that Slt2 may control Npr1-regulated residues in some proteins indirectly via a protein phosphatase (similar to Yak1 and the Gwl pathway above) or by inhibiting another protein kinase. In this context, our phosphoproteome data pinpointed Gip3, a protein phosphatase 1 (PP1) regulator (Pinsky et al., 2006), as a potential Slt2 target. Loss of Gip3, however, did not noticeably alter the electrophoretic mobility (on phostag gels) of the shared Npr1/Slt2 targets Chs5, Tif11, and Sec7 when extracted from rapamycin-treated cells. In control experiments, however, we noticed that the rapamycin-induced dephosphorylation of Npr1 (Schmidt et al., 1998), which was visualized by an increase in Npr1 electrophoretic mobility, significantly depended on the presence of Slt2 (Figure S2A). In line with these findings, our phosphoproteome data also revealed the presence of four rapamycin-sensitive serine residues in the N-terminal part of Npr1 that required the presence of Slt2 to be dephosphorylated upon TORC1 inactivation (Figure S2B). Thus, Slt2 indirectly controls the phosphorylation state of Npr1 by activating or inhibiting an unknown protein phosphatase or kinase, respectively.

Npr1 controls the rate of autophagosome assembly via Atg9

To also validate the data from our Npr1-controlled phosphoproteome, we next addressed the possibility that Npr1 may modulate macroautophagy by phosphorylating Ser^{122} within the conserved transmembrane protein and integral unit of the core macroautophagy machinery Atg9 (Noda et al., 2000). Notably, Atg1-independent Atg9-Ser^{122} phosphorylation by an unknown kinase controls the movement of Atg9 from peripheral sites to the phagophore assembly site (PAS) and hence stimulates the rate of autophagosome formation (Feng et al., 2016). In control experiments, we confirmed that both the colocalization of Atg9-GFP with the PAS marker BFP-Ape1 and macroautophagic flux were significantly reduced or enhanced by introduction of Ser^{122}-Ala (Atg9^{S122A}-GFP) or phosphomimetic Ser^{122}-Asp (Atg9^{S122D}-GFP) mutations in Atg9, respectively (Figures 5A–5C). Interestingly, while loss of Npr1 diminished both the colocalization of Atg9-GFP with BFP-Ape1 and macroautopagic flux comparably to the Ser^{122}-Ala mutation in Atg9, the Ser^{122}-Asp mutation in Atg9 fully reversed these effects, which indicates that Npr1 may control macroautophagy primarily through phosphorylation of Ser^{122} in Atg9. In line with this reasoning, our *in vitro* kinase assays using purified kinase and substrate also confirmed that Npr1 can directly phosphorylate Atg9-Ser^{122} (Figure 5D). Thus, Npr1-mediated phosphorylation of Atg9-Ser^{122} stimulates the rate of autophagosome formation by favoring the association of Atg9 vesicles with the PAS during macroautophagy. Notably, following recruitment of Atg9 to the PAS, it can then be phosphorylated by Atg1 (on Ser^{19}, Ser^{657}, Ser^{802}, Ser^{831}, Ser^{948}, and Ser^{969}, of which our Atg1-dependent phosphoproteome also identified Ser^{802} and Ser^{969}), which then allows efficient recruitment of Atg8 and Atg18, which are required for subsequent steps of macroautophagy (e.g., the isolation membrane elongation) (Papinski et al., 2014) (Figure 5E).

Distal protein kinases engage in multilayered TORC1 feedback control circuits

TORC1 often operates in the context of feedback loops, which enable it to maintain various aspects of cellular homeostasis (Eltschinger and Loewith, 2016). In this context, our phosphoproteome data also provide a wealth of leads that may help untangle the architecture of these built-in feedback mechanisms that are still incompletely understood. For instance, Npr1 may phosphorylate the putative amino acid sensor and phosphatidylinositol-3-phosphate binding protein Pib2 to mediate an earlier proposed TORC1 feedback control mechanism (Brito et al., 2019; Michel et al., 2017; Tanigawa and Maeda, 2017) (Figure S3A). In a similar vein, Npr1 may also phosphorylate the presumed Psr1/2 phosphatase regulator Whi2, which negatively controls TORC1 via a still poorly defined means (Chen et al., 2018; Teng et al., 2018) (Figure S3B). Moreover, the PKA signaling pathway may receive inputs via Atg1 (on Gpa2) and Yak1 (on Bcy1), which could serve to control TORC1 through Rim15-dependent phosphorylation of the protein kinase Ksp1 that reportedly inhibits macroautophagy by activating TORC1 (Umekawa and Klionsky, 2012) (Figure S3C). Finally, our data also pinpoint a possible role of Yak1 in phosphorylating the TORC1 subunit Tco89 and of Atg1 in phosphorylating the Seh1 subunit of SEACAT (i.e., the SEA complex that activates TORC1), which regulates TORC1 indirectly through the Rag GTPases (Panchaud et al., 2013) (Figures S3D and S3E). Combined, our data therefore indicate the existence of a multilayered regulatory network that engages distal effector kinases in complex feedback loops and thus provide a framework for future studies aimed at deciphering the mechanisms that enable TORC1 to ensure robust and homeostatic cellular responses.

Sch9 may antagonize the quiescence program in part through Mck1

The proximal TORC1 effector Sch9 stimulates growth by promoting Ribi, ribosomal protein (RP) gene expression, and RNA polymerase III-dependent transcription mainly via phosphorylation of a set of transcriptional repressors including Stb3, Dot6, Tod6, and Maf1 (Albert et al., 2016; Huber et al., 2009, 2011; Yabuki et al., 2019). In a similar vein, it sustains fermentative growth by phosphorylation of the transcription factor Hcm1 (Deprez et al., 2018; Rodríguez-Colman et al., 2013). In parallel, Sch9 plays a key role in preventing the induction of specific aspects of the quiescence program through inhibition of Rim15, Slt2, and Yak1 (Figure 1). Whether Sch9 may antagonize the quiescence program by inhibiting protein kinases other than Rim15, Slt2, and Yak1 is currently not known. To address this question, we reanalyzed a recently published phosphoproteome dataset, which served to identify proximal Sch9 targets that are hypophosphorylated following acute inhibition of an ATP-analog-sensitive Sch9^{as} allele (Plank et al., 2020). Accordingly, we were able to extract 121 residues that were oppositely regulated (i.e., hyper-phosphorylated) upon inactivation of Sch9 and that we were able to match with phospho-residues in our current study (Table S3; Figure S4A). Among these residues, 39 were also

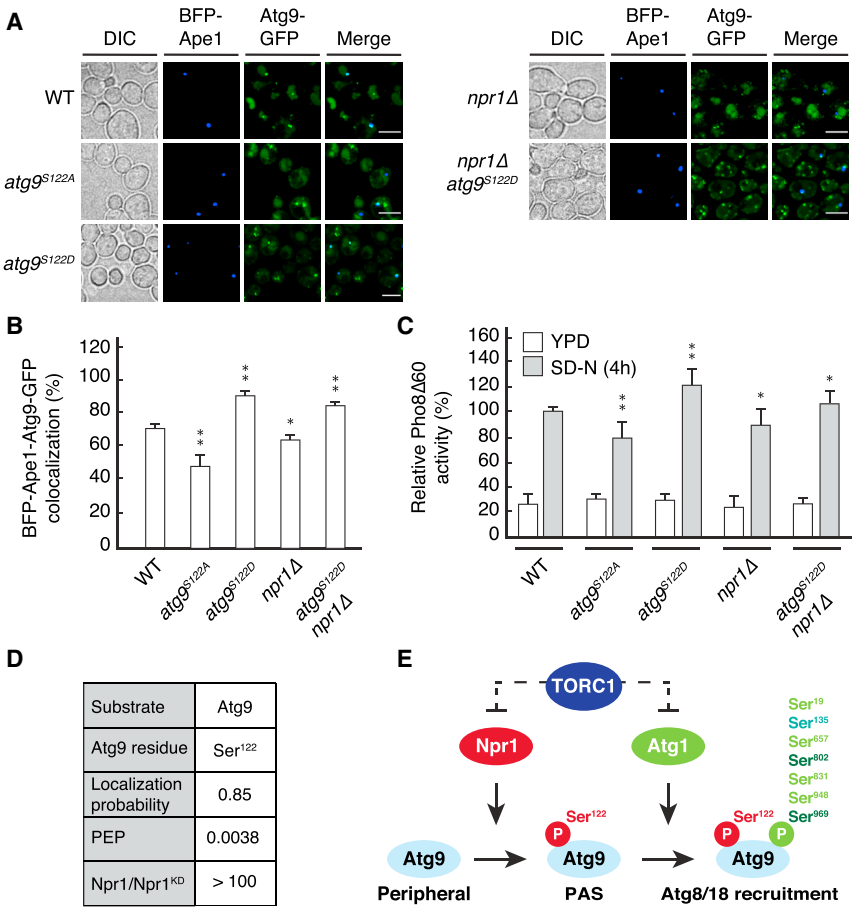

Figure 5. Npr1 controls the rate of autophagosome assembly by phosphorylation of Atg9-Ser^{122}

(A) Representative fluorescence microscopy images of wild-type (WT) and indicated mutant cells expressing Atg9-GFP variants and plasmid-encoded BFP-Ape1. Cells were cultured in SD (synthetic defined) medium lacking histidine and then starved for nitrogen for 30 min. Scale bars: 5 μm.

(B) Quantification of colocalization between Atg9-GFP variants and BFP-Ape1. For each strain, at least 80 cells were recorded (n = 3; +SD; data are presented as means). Unpaired Student's t tests were used to determine significant differences in (B) and (C) when compared to the respective WT control (*p ≤ 0.05; **p ≤ 0.001; ***p ≤ 0.0001). Colocalization in *npr1*Δ and *npr1*Δ *atg9*^{S122D} is significantly different (p = 0.0002).

(C) WT and indicated mutant cells (all *pho8Δ60*) were grown exponentially in YPD (yeast extract-peptone-dextrose) and then shifted to SD-N for 4 h. Pho8Δ60 phosphatase activities were normalized to the ones of nitrogen-starved WT cells (100%; n = 6; +SD; data are presented as means). Macroautophagy flux in *npr1*Δ and *npr1*Δ *atg9*^{S122D} is significantly different (p = 0.0192).

(D) *In vitro* phosphorylation of Atg9 by Npr1. Recombinant Atg9 was subjected to *in vitro* kinase assays using GST-Npr1 or kinase-dead GST-Npr1^{K467R} (Npr1^{KD}). The phosphorylation level of Ser^{122} in Atg9 was compared between samples treated with GST-Npr1 or GST-Npr1^{KD}. Localization probabilities and posterior error probabilities (PEP) are indicated.

(E) Model for the regulation of Atg9 by Npr1 and Atg1. Solid arrows refer to direct interactions; dashed bars refer to indirect interactions. Of the previously identified six Atg1 target residues in Atg9 (light and dark green numbered serines [Ser]), we identified here Ser^{802} and Ser^{969} (dark green). In addition, we also identified Ser^{135} (turquoise) as a potential Atg1 target residue in Atg9. For details, see text.

significantly hyperphosphorylated in rapamycin-treated wild-type cells and hence fulfilled the criteria for being potentially phosphorylated by an Sch9-inhibited effector kinase(s). While 77% (or 30 of 39) of these residues were controlled by Rim15, Slt2, and/or Yak1 as expected, 23% (or 9 of 39) appeared indeed to be controlled through at least one other kinase (Figure S4A). Intriguingly, a motif analysis indicated that the majority of these remaining phospho-sites perfectly matched the consensus motif predicted to be targeted by the glycogen synthase kinase-3 (GSK-3) (i.e., [S/T]XXXpS/pT where the +4pS/pT represent priming sites for GSK-3-dependent phosphorylation [Kaidanovich-Beilin and Woodgett, 2011; Sutherland, 2011]) (Figure S4B). Combined with the independent observations that Mck1, one of four GSK-3 orthologs in yeast (Kassir et al., 2006), (1) functions downstream of TORC1 (Lee et al., 2012), (2) mediates the slow growth of *sch9Δ* cells (Peterson and Liu, 2021), and (3) stimulates the quiescence program in parallel to Rim15 and Yak1 (Cao et al., 2016; Quan et al., 2015), our analyses therefore suggest that TORC1 inhibits the quiescence program in part via Sch9-dependent inhibition of Mck1. Furthermore, this potentially linear pathway may be evolutionarily conserved, as mTORC1 inhibits GSK-3 via the ribosomal protein S6 kinase (S6K1) (Zhang et al., 2006), and hence warrants future studies.

Evolutionary conservation of distally controlled TORC1 effector kinases

Yak1 is a founding member of the highly conserved DYRK family that hosts several mammalian orthologs (Aranda et al., 2011). Interestingly, mammalian DYRK kinases regulate various processes including cell cycle, cell proliferation, differentiation, and quiescence and consequently play a role in a broad spectrum of both physiological and pathological processes such as muscle development, erythropoiesis, neurodegeneration, tumorigenesis, and cancer (Abbassi et al., 2015; Soppa and Becker, 2015). Likewise, Rim15 is orthologous to the Gwl kinases in higher eukaryotes that control cell cycle, mitosis, meiotic maturation, DNA replication, and cancer (Castro and Lorca, 2018). Npr1 and Slt2, in contrast, do not have clear orthologs in mammals, although Slt2 shares significant sequence similarities with several MAPKs. Consequently, we deem it possible that some of our identified Yak1 and Rim15 substrates may be subjected to evolutionarily conserved control mechanisms. We therefore retrieved the human orthologs of our Yak1 and Rim15 targets and were able to identify several highly conserved residues in effector proteins that are commonly or separately regulated by Rim15 and Yak1 (Figure S5). These include, for instance, the Mih1/MPIP3 protein phosphatase that is involved

in cell cycle regulation, the Rph1/KDM4C histone demethylase, the Rsc1/PB1 chromatin remodeling complex subunit, and the translation initiation factor eIF4G (Tif4632/IF43G) that may be key for proper control of various DYRK- and/or Gwl-dependent processes. Thus, our data may also serve to guide future research in mammalian cells.

Limitations of the study

With respect to the chosen data-dependent phosphoproteomic analyses, the following limitations apply. Because of the partially stochastic, intensity-based selection of peptides for fragmentation by MS/MS, datasets generated in different SILAC experiments may vary with respect to the sequenced phosphopeptides. This leads to missing values and incomplete data matrices when several SILAC experiments are merged; in our case, 17 datasets per KoI. However, compared to other types of analyses, the absence of a datapoint in a specific experiment cannot be interpreted as no or low signal. Missing values have to be disregarded, i.e., treated as "not determined." Missing values in combination with the noise of phosphopeptide analyses might lead to the exclusion of biologically meaningful hits. In addition, some phosphosites might have only been quantified in multiply phosphorylated peptides. In such cases, one cannot determine which of the sites, a single one or a combination, are regulated.

STAR★METHODS

Detailed methods are provided in the online version of this paper and include the following:

- KEY RESOURCES TABLE
- RESOURCE AVAILABILITY
  - Lead contact
  - Materials availability
  - Data and code availability
- EXPERIMENTAL MODEL AND SUBJECT DETAILS
- METHOD DETAILS
  - Yeast strains, plasmids, and growth conditions
  - MS sample preparation, phosphopeptide enrichment, and LC-MS/MS and data analyses
  - Protein purification and Npr1 *in vitro* kinase assay
  - Cell lysate preparation and immunoblot analysis
  - β-galactosidase assays
  - Fluorescence microscopy
  - ALP assays
- QUANTIFICATION AND STATISTICAL ANALYSIS

SUPPLEMENTAL INFORMATION

Supplemental information can be found online at https://doi.org/10.1016/j.celrep.2021.110149.

ACKNOWLEDGMENTS

We thank Susanne Stumpe for technical assistance, Dan Klionsky and Michael Hall for strains and plasmids, Marco Visani for providing the MV_pairwise_alignment program, and Claudine Kraft for insightful comments. This work was supported by the Canton of Fribourg (to J.D. and C.D.V.), the Swiss National Science Foundation (310030_166474/184671 to C.D.V. and 310030_184781 and 316030_177088 to J.D.) and the Novartis Foundation for Medical-Biological Research (to C.D.V.)

AUTHOR CONTRIBUTIONS

Conceptualization, J.D. and C.D.V.; methodology, L.D., M.S., Z.H., J.D., and C.D.V.; investigation, L.D., M.S., Z.H., and M.J.; writing – original draft, J.D. and C.D.V.; writing – review & editing, L.D., J.D., and C.D.V.; funding acquisition, resources, & supervision, J.D. and C.D.V.

DECLARATION OF INTERESTS

The authors declare no competing interests.

Received: July 27, 2021
Revised: October 19, 2021
Accepted: November 30, 2021
Published: December 28, 2021

REFERENCES

Abbassi, R., Johns, T.G., Kassiou, M., and Munoz, L. (2015). DYRK1A in neurodegeneration and cancer: Molecular basis and clinical implications. Pharmacol. Ther. *151*, 87–98.

Ai, W., Bertram, P.G., Tsang, C.K., Chan, T.F., and Zheng, X.F. (2002). Regulation of subtelomeric silencing during stress response. Mol. Cell *10*, 1295–1305.

Albert, B., Knight, B., Merwin, J., Martin, V., Ottoz, D., Gloor, Y., Bruzzone, M.J., Rudner, A., and Shore, D. (2016). A molecular titration system coordinates ribosomal protein gene transcription with ribosomal RNA synthesis. Mol. Cell *64*, 720–733.

Annan, R.B., Wu, C., Waller, D.D., Whiteway, M., and Thomas, D.Y. (2008). Rho5p is involved in mediating the osmotic stress response in *Saccharomyces cerevisiae*, and its activity is regulated via Msi1p and Npr1p by phosphorylation and ubiquitination. Eukaryot. Cell *7*, 1441–1449.

Aranda, S., Laguna, A., and de la Luna, S. (2011). DYRK family of protein kinases: evolutionary relationships, biochemical properties, and functional roles. FASEB J. *25*, 449–462.

Baro, B., Játiva, S., Calabria, I., Vinaixa, J., Bech-Serra, J.J., de LaTorre, C., Rodrigues, J., Hernáez, M.L., Gil, C., Barceló-Batllori, S., et al. (2018). SILAC-based phosphoproteomics reveals new PP2A-Cdc55-regulated processes in budding yeast. Gigascience *7*, 1–18.

Bernard, A., Jin, M., González-Rodríguez, P., Füllgrabe, J., Delorme-Axford, E., Backues, S.K., Joseph, B., and Klionsky, D.J. (2015). Rph1/KDM4 mediates nutrient-limitation signaling that leads to the transcriptional induction of autophagy. Curr. Biol. *25*, 546–555.

Binda, M., Péli-Gulli, M.P., Bonfils, G., Panchaud, N., Urban, J., Sturgill, T.W., Loewith, R., and De Virgilio, C. (2009). The Vam6 GEF controls TORC1 by activating the EGO complex. Mol. Cell *35*, 563–573.

Bindea, G., Mlecnik, B., Hackl, H., Charoentong, P., Tosolini, M., Kirilovsky, A., Fridman, W.H., Pagès, F., Trajanoski, Z., and Galon, J. (2009). ClueGO: a Cytoscape plug-in to decipher functionally grouped gene ontology and pathway annotation networks. Bioinformatics *25*, 1091–1093.

Boeckstaens, M., Llinares, E., Van Vooren, P., and Marini, A.M. (2014). The TORC1 effector kinase Npr1 fine tunes the inherent activity of the Mep2 ammonium transport protein. Nat. Commun. *5*, 3101.

Boeckstaens, M., Merhi, A., Llinares, E., Van Vooren, P., Springael, J.Y., Wintjens, R., and Marini, A.M. (2015). Identification of a novel regulatory mechanism of nutrient transport controlled by TORC1-Npr1-Amu1/Par32. PLoS Genet. *11*, e1005382.

Bonenfant, D., Schmelzle, T., Jacinto, E., Crespo, J.L., Mini, T., Hall, M.N., and Jenoe, P. (2003). Quantitation of changes in protein phosphorylation: a simple method based on stable isotope labeling and mass spectrometry. Proc. Natl. Acad. Sci. USA *100*, 880–885.

Bontron, S., Jaquenoud, M., Vaga, S., Talarek, N., Bodenmiller, B., Aebersold, R., and De Virgilio, C. (2013). Yeast endosulfines control entry into quiescence and chronological life span by inhibiting protein phosphatase 2A. Cell Rep. *3*, 16–22.

Boorstein, W.R., and Craig, E.A. (1990). Regulation of a yeast HSP70 gene by a cAMP responsive transcriptional control element. EMBO J. *9*, 2543–2553.

Brachmann, C.B., Davies, A., Cost, G.J., Caputo, E., Li, J., Hieter, P., and Boeke, J.D. (1998). Designer deletion strains derived from *Saccharomyces cerevisiae* S288C: a useful set of strains and plasmids for PCR-mediated gene disruption and other applications. Yeast *14*, 115–132.

Breslow, D.K., Collins, S.R., Bodenmiller, B., Aebersold, R., Simons, K., Shevchenko, A., Ejsing, C.S., and Weissman, J.S. (2010). Orm family proteins mediate sphingolipid homeostasis. Nature *463*, 1048–1053.

Brito, A.S., Soto Diaz, S., Van Vooren, P., Godard, P., Marini, A.M., and Boeckstaens, M. (2019). Pib2-dependent feedback control of the TORC1 signaling network by the Npr1 kinase. iScience *20*, 415–433.

Cao, L., Tang, Y., Quan, Z., Zhang, Z., Oliver, S.G., and Zhang, N. (2016). Chronological lifespan in yeast is dependent on the accumulation of storage carbohydrates mediated by Yak1, Mck1 and Rim15 kinases. PLoS Genet. *12*, e1006458.

Castro, A., and Lorca, T. (2018). Greatwall kinase at a glance. J. Cell Sci. *131*, jcs222364.

Chen, X., Wang, G., Zhang, Y., Dayhoff-Brannigan, M., Diny, N.L., Zhao, M., He, G., Sing, C.N., Metz, K.A., Stolp, Z.D., et al. (2018). Whi2 is a conserved negative regulator of TORC1 in response to low amino acids. PLoS Genet. *14*, e1007592.

Chen, Z., Malia, P.C., Hatakeyama, R., Nicastro, R., Hu, Z., Péli-Gulli, M.P., Gao, J., Nishimura, T., Eskes, E., Stefan, C.J., et al. (2021). TORC1 determines Fab1 lipid kinase function at signaling endosomes and vacuoles. Curr. Biol. *31*, 297–309.e8.

Cherkasova, V.A., and Hinnebusch, A.G. (2003). Translational control by TOR and TAP42 through dephosphorylation of eIF2alpha kinase GCN2. Genes Dev. *17*, 859–872.

Cornu, M., Albert, V., and Hall, M.N. (2013). mTOR in aging, metabolism, and cancer. Curr. Opin. Genet. Dev. *23*, 53–62.

Cox, J., and Mann, M. (2008). MaxQuant enables high peptide identification rates, individualized p.p.b.-range mass accuracies and proteome-wide protein quantification. Nat. Biotechnol. *26*, 1367–1372.

Crooks, G.E., Hon, G., Chandonia, J.M., and Brenner, S.E. (2004). WebLogo: a sequence logo generator. Genome Res. *14*, 1188–1190.

De Craene, J.O., Soetens, O., and Andre, B. (2001). The Npr1 kinase controls biosynthetic and endocytic sorting of the yeast Gap1 permease. J. Biol. Chem. *276*, 43939–43948.

De Virgilio, C. (2012). The essence of yeast quiescence. FEMS Microbiol. Rev. *36*, 306–339.

Deprez, M.A., Eskes, E., Winderickx, J., and Wilms, T. (2018). The TORC1-Sch9 pathway as a crucial mediator of chronological lifespan in the yeast *Saccharomyces cerevisiae*. FEMS Yeast Res. *18*. https://doi.org/10.1093/femsyr/foy048.

Di Como, C.J., and Arndt, K.T. (1996). Nutrients, via the Tor proteins, stimulate the association of Tap42 with type 2A phosphatases. Genes Dev. *10*, 1904–1916.

Dokládal, L., Stumpe, M., Pillet, B., Hu, Z., Garcia Osuna, G.M., Kressler, D., Dengjel, J., and De Virgilio, C. (2021). Global phosphoproteomics pinpoints uncharted Gcn2-mediated mechanisms of translational control. Mol. Cell *81*, 1879–1889.e6.

Drummond, D.A., Bloom, J.D., Adami, C., Wilke, C.O., and Arnold, F.H. (2005). Why highly expressed proteins evolve slowly. Proc. Natl. Acad. Sci. USA *102*, 14338–14343.

Eltschinger, S., and Loewith, R. (2016). TOR complexes and the maintenance of cellular homeostasis. Trends Cell Biol. *26*, 148–159.

Feng, Y., Backues, S.K., Baba, M., Heo, J.M., Harper, J.W., and Klionsky, D.J. (2016). Phosphorylation of Atg9 regulates movement to the phagophore assembly site and the rate of autophagosome formation. Autophagy *12*, 648–658.

Gander, S., Bonenfant, D., Altermatt, P., Martin, D.E., Hauri, S., Moes, S., Hall, M.N., and Jenoe, P. (2008). Identification of the rapamycin-sensitive phosphorylation sites within the Ser/Thr-rich domain of the yeast Npr1 protein kinase. Rapid Commun. Mass Spectrom. *22*, 3743–3753.

Garrett, S., Menold, M.M., and Broach, J.R. (1991). The *Saccharomyces cerevisiae YAK1* gene encodes a protein kinase that is induced by arrest early in the cell cycle. Mol. Cell. Biol. *11*, 4045–4052.

Generoso, W.C., Gottardi, M., Oreb, M., and Boles, E. (2016). Simplified CRISPR-Cas genome editing for *Saccharomyces cerevisiae*. J. Microbiol. Methods *127*, 203–205.

Gharbi-Ayachi, A., Labbé, J.C., Burgess, A., Vigneron, S., Strub, J.M., Brioudes, E., Van-Dorsselaer, A., Castro, A., and Lorca, T. (2010). The substrate of Greatwall kinase, Arpp19, controls mitosis by inhibiting protein phosphatase 2A. Science *330*, 1673–1677.

Godfrey, M., Touati, S.A., Kataria, M., Jones, A., Snijders, A.P., and Uhlmann, F. (2017). PP2A^{Cdc55} phosphatase imposes ordered cell-cycle phosphorylation by opposing threonine phosphorylation. Mol. Cell *65*, 393–402.e3.

Goldman, A., Roy, J., Bodenmiller, B., Wanka, S., Landry, C.R., Aebersold, R., and Cyert, M.S. (2014). The calcineurin signaling network evolves via conserved kinase-phosphatase modules that transcend substrate identity. Mol. Cell *55*, 422–435.

González, A., and Hall, M.N. (2017). Nutrient sensing and TOR signaling in yeast and mammals. EMBO J. *36*, 397–408.

González, A., Shimobayashi, M., Eisenberg, T., Merle, D.A., Pendl, T., Hall, M.N., and Moustafa, T. (2015). TORC1 promotes phosphorylation of ribosomal protein S6 via the AGC kinase Ypk3 in *Saccharomyces cerevisiae*. PLoS ONE *10*, e0120250.

Griffioen, G., Branduardi, P., Ballarini, A., Anghileri, P., Norbeck, J., Baroni, M.D., and Ruis, H. (2001). Nucleocytoplasmic distribution of budding yeast protein kinase A regulatory subunit Bcy1 requires Zds1 and is regulated by Yak1-dependent phosphorylation of its targeting domain. Mol. Cell. Biol. *21*, 511–523.

Guarente, L. (1983). Yeast promoters and *lacZ* fusions designed to study expression of cloned genes in yeast. Methods Enzymol. *101*, 181–191.

Harrison, J.C., Zyla, T.R., Bardes, E.S., and Lew, D.J. (2004). Stress-specific activation mechanisms for the "cell integrity" MAPK pathway. J. Biol. Chem. *279*, 2616–2622.

Hatakeyama, R., Péli-Gulli, M.P., Hu, Z., Jaquenoud, M., Garcia Osuna, G.M., Sardu, A., Dengjel, J., and De Virgilio, C. (2019). Spatially distinct pools of TORC1 balance protein homeostasis. Mol. Cell *73*, 325–338.e8.

Hinnebusch, A.G. (2005). Translational regulation of *GCN4* and the general amino acid control of yeast. Annu. Rev. Microbiol. *59*, 407–450.

Hu, Z., Raucci, S., Jaquenoud, M., Hatakeyama, R., Stumpe, M., Rohr, R., Reggiori, F., De Virgilio, C., and Dengjel, J. (2019). Multilayered control of protein turnover by TORC1 and Atg1. Cell Rep. *28*, 3486–3496.e6.

Huber, A., Bodenmiller, B., Uotila, A., Stahl, M., Wanka, S., Gerrits, B., Aebersold, R., and Loewith, R. (2009). Characterization of the rapamycin-sensitive phosphoproteome reveals that Sch9 is a central coordinator of protein synthesis. Genes Dev. *23*, 1929–1943.

Huber, A., French, S.L., Tekotte, H., Yerlikaya, S., Stahl, M., Perepelkina, M.P., Tyers, M., Rougemont, J., Beyer, A.L., and Loewith, R. (2011). Sch9 regulates ribosome biogenesis via Stb3, Dot6 and Tod6 and the histone deacetylase complex RPD3L. EMBO J. *30*, 3052–3064.

Jacinto, E., Guo, B., Arndt, K.T., Schmelzle, T., and Hall, M.N. (2001). TIP41 interacts with TAP42 and negatively regulates the TOR signaling pathway. Mol. Cell *8*, 1017–1026.

Janke, C., Magiera, M.M., Rathfelder, N., Taxis, C., Reber, S., Maekawa, H., Moreno-Borchart, A., Doenges, G., Schwob, E., Schiebel, E., and Knop, M. (2004). A versatile toolbox for PCR-based tagging of yeast genes: new fluorescent proteins, more markers and promoter substitution cassettes. Yeast *21*, 947–962.

Jiang, Y., and Broach, J.R. (1999). Tor proteins and protein phosphatase 2A reciprocally regulate Tap42 in controlling cell growth in yeast. EMBO J. *18*, 2782–2792.

Jiménez-Gutiérrez, E., Alegría-Carrasco, E., Sellers-Moya, Á., Molina, M., and Martín, H. (2020). Not just the wall: the other ways to turn the yeast CWI pathway on. Int. Microbiol. *23*, 107–119.

Jorgensen, P., Rupes, I., Sharom, J.R., Schneper, L., Broach, J.R., and Tyers, M. (2004). A dynamic transcriptional network communicates growth potential to ribosome synthesis and critical cell size. Genes Dev. *18*, 2491–2505.

Kaidanovich-Beilin, O., and Woodgett, J.R. (2011). GSK-3: Functional Insights from Cell Biology and Animal Models. Front. Mol. Neurosci. *4*, 40.

Kamada, Y., Yoshino, K., Kondo, C., Kawamata, T., Oshiro, N., Yonezawa, K., and Ohsumi, Y. (2010). Tor directly controls the Atg1 kinase complex to regulate autophagy. Mol. Cell. Biol. *30*, 1049–1058.

Kassir, Y., Rubin-Bejerano, I., and Mandel-Gutfreund, Y. (2006). The Saccharomyces cerevisiae GSK-3 β homologs. Curr. Drug Targets *7*, 1455–1465.

Kim, E.M., Kim, J., Kim, Y.G., Lee, P., Shin, D.S., Kim, M., Hahn, J.S., Lee, Y.S., and Kim, B.G. (2011). Development of high-throughput phosphorylation profiling method for identification of Ser/Thr kinase specificity. J. Pept. Sci. *17*, 392–397.

Klionsky, D.J., Abdel-Aziz, A.K., Abdelfatah, S., Abdellatif, M., Abdoli, A., Abel, S., Abeliovich, H., Abildgaard, M.H., Abudu, Y.P., Acevedo-Arozena, A., et al. (2021). Guidelines for the use and interpretation of assays for monitoring autophagy (4th edition)[1]. Autophagy *17*, 1–382.

Krause, S.A., and Gray, J.V. (2002). The protein kinase C pathway is required for viability in quiescence in *Saccharomyces cerevisiae*. Curr. Biol. *12*, 588–593.

Kuranda, K., Leberre, V., Sokol, S., Palamarczyk, G., and François, J. (2006). Investigating the caffeine effects in the yeast *Saccharomyces cerevisiae* brings new insights into the connection between TOR, PKC and Ras/cAMP signalling pathways. Mol. Microbiol. *61*, 1147–1166.

Lee, P., Cho, B.R., Joo, H.S., and Hahn, J.S. (2008). Yeast Yak1 kinase, a bridge between PKA and stress-responsive transcription factors, Hsf1 and Msn2/Msn4. Mol. Microbiol. *70*, 882–895.

Lee, J., Moir, R.D., and Willis, I.M. (2009). Regulation of RNA polymerase III transcription involves *SCH9*-dependent and *SCH9*-independent branches of the target of rapamycin (TOR) pathway. J. Biol. Chem. *284*, 12604–12608.

Lee, P., Paik, S.-M., Shin, C.-S., Huh, W.-K., and Hahn, J.S. (2011). Regulation of yeast Yak1 kinase by PKA and autophosphorylation-dependent 14-3-3 binding. Mol. Microbiol. *79*, 633–646.

Lee, J., Moir, R.D., McIntosh, K.B., and Willis, I.M. (2012). TOR signaling regulates ribosome and tRNA synthesis via LAMMER/Clk and GSK-3 family kinases. Mol. Cell *45*, 836–843.

Lee, P., Kim, M.S., Paik, S.M., Choi, S.H., Cho, B.R., and Hahn, J.S. (2013). Rim15-dependent activation of Hsf1 and Msn2/4 transcription factors by direct phosphorylation in *Saccharomyces cerevisiae*. FEBS Lett. *587*, 3648–3655.

Lempiäinen, H., Uotila, A., Urban, J., Dohnal, I., Ammerer, G., Loewith, R., and Shore, D. (2009). Sfp1 interaction with TORC1 and Mrs6 reveals feedback regulation on TOR signaling. Mol. Cell *33*, 704–716.

Levin, D.E. (2005). Cell wall integrity signaling in *Saccharomyces cerevisiae*. Microbiol. Mol. Biol. Rev. *69*, 262–291.

Li, J., Paulo, J.A., Nusinow, D.P., Huttlin, E.L., and Gygi, S.P. (2019). Investigation of proteomic and phosphoproteomic responses to signaling network perturbations reveals functional pathway organizations in yeast. Cell Rep. *29*, 2092–2104.e4.

Li, T., Huang, T., Du, M., Chen, X., Du, F., Ren, J., and Chen, Z.J. (2021). Phosphorylation and chromatin tethering prevent cGAS activation during mitosis. Science *371*, eabc5386.

Liu, G.Y., and Sabatini, D.M. (2020). mTOR at the nexus of nutrition, growth, ageing and disease. Nat. Rev. Mol. Cell Biol. *21*, 183–203.

Loewith, R., and Hall, M.N. (2011). Target of rapamycin (TOR) in nutrient signaling and growth control. Genetics *189*, 1177–1201.

MacGurn, J.A., Hsu, P.C., Smolka, M.B., and Emr, S.D. (2011). TORC1 regulates endocytosis via Npr1-mediated phosphoinhibition of a ubiquitin ligase adaptor. Cell *147*, 1104–1117.

Malcher, M., Schladebeck, S., and Mösch, H.U. (2011). The Yak1 protein kinase lies at the center of a regulatory cascade affecting adhesive growth and stress resistance in *Saccharomyces cerevisiae*. Genetics *187*, 717–730.

Malys, N., Carroll, K., Miyan, J., Tollervey, D., and McCarthy, J.E. (2004). The 'scavenger' m^7GpppX pyrophosphatase activity of Dcs1 modulates nutrient-induced responses in yeast. Nucleic Acids Res. *32*, 3590–3600.

Martin, D.E., Soulard, A., and Hall, M.N. (2004). TOR regulates ribosomal protein gene expression via PKA and the Forkhead transcription factor FHL1. Cell *119*, 969–979.

Merhi, A., and André, B. (2012). Internal amino acids promote Gap1 permease ubiquitylation via TORC1/Npr1/14-3-3-dependent control of the Bul arrestin-like adaptors. Mol. Cell. Biol. *32*, 4510–4522.

Michel, A.H., Hatakeyama, R., Kimmig, P., Arter, M., Peter, M., Matos, J., De Virgilio, C., and Kornmann, B. (2017). Functional mapping of yeast genomes by saturated transposition. eLife *6*, e23570.

Mishra, R., van Drogen, F., Dechant, R., Oh, S., Jeon, N.L., Lee, S.S., and Peter, M. (2017). Protein kinase C and calcineurin cooperatively mediate cell survival under compressive mechanical stress. Proc. Natl. Acad. Sci. USA *114*, 13471–13476.

Mizushima, N., Yoshimori, T., and Ohsumi, Y. (2011). The role of Atg proteins in autophagosome formation. Annu. Rev. Cell Dev. Biol. *27*, 107–132.

Mochida, S., Maslen, S.L., Skehel, M., and Hunt, T. (2010). Greatwall phosphorylates an inhibitor of protein phosphatase 2A that is essential for mitosis. Science *330*, 1670–1673.

Mok, J., Kim, P.M., Lam, H.Y., Piccirillo, S., Zhou, X., Jeschke, G.R., Sheridan, D.L., Parker, S.A., Desai, V., Jwa, M., et al. (2010). Deciphering protein kinase specificity through large-scale analysis of yeast phosphorylation site motifs. Sci. Signal. *3*, ra12.

Moreno-Torres, M., Jaquenoud, M., and De Virgilio, C. (2015). TORC1 controls G_1-S cell cycle transition in yeast via Mpk1 and the greatwall kinase pathway. Nat. Commun. *6*, 8256.

Moreno-Torres, M., Jaquenoud, M., Péli-Gulli, M.P., Nicastro, R., and De Virgilio, C. (2017). TORC1 coordinates the conversion of Sic1 from a target to an inhibitor of cyclin-CDK-Cks1. Cell Discov. *3*, 17012.

Moriya, H., Shimizu-Yoshida, Y., Omori, A., Iwashita, S., Katoh, M., and Sakai, A. (2001). Yak1p, a DYRK family kinase, translocates to the nucleus and phosphorylates yeast Pop2p in response to a glucose signal. Genes Dev. *15*, 1217–1228.

Noda, T., Matsuura, A., Wada, Y., and Ohsumi, Y. (1995). Novel system for monitoring autophagy in the yeast *Saccharomyces cerevisiae*. Biochem. Biophys. Res. Commun. *210*, 126–132.

Noda, T., Kim, J., Huang, W.P., Baba, M., Tokunaga, C., Ohsumi, Y., and Klionsky, D.J. (2000). Apg9p/Cvt7p is an integral membrane protein required for transport vesicle formation in the Cvt and autophagy pathways. J. Cell Biol. *148*, 465–480.

Olsen, J.V., Blagoev, B., Gnad, F., Macek, B., Kumar, C., Mortensen, P., and Mann, M. (2006). Global, in vivo, and site-specific phosphorylation dynamics in signaling networks. Cell *127*, 635–648.

Panchaud, N., Péli-Gulli, M.P., and De Virgilio, C. (2013). SEACing the GAP that nEGOCiates TORC1 activation: evolutionary conservation of Rag GTPase regulation. Cell Cycle *12*, 2948–2952.

Papinski, D., Schuschnig, M., Reiter, W., Wilhelm, L., Barnes, C.A., Maiolica, A., Hansmann, I., Pfaffenwimmer, T., Kijanska, M., Stoffel, I., et al. (2014). Early steps in autophagy depend on direct phosphorylation of Atg9 by the Atg1 kinase. Mol. Cell *53*, 471–483.

Pedruzzi, I., Bürckert, N., Egger, P., and De Virgilio, C. (2000). *Saccharomyces cerevisiae* Ras/cAMP pathway controls post-diauxic shift element-dependent transcription through the zinc finger protein Gis1. EMBO J. *19*, 2569–2579.

Pedruzzi, I., Dubouloz, F., Cameroni, E., Wanke, V., Roosen, J., Winderickx, J., and De Virgilio, C. (2003). TOR and PKA signaling pathways converge on the protein kinase Rim15 to control entry into G_0. Mol. Cell *12*, 1607–1613.

Péli-Gulli, M.P., Raucci, S., Hu, Z., Dengjel, J., and De Virgilio, C. (2017). Feedback inhibition of the Rag GTPase GAP complex Lst4-Lst7 safeguards TORC1 from hyperactivation by amino acid signals. Cell Rep. *20*, 281–288.

Perez-Riverol, Y., Csordas, A., Bai, J., Bernal-Llinares, M., Hewapathirana, S., Kundu, D.J., Inuganti, A., Griss, J., Mayer, G., Eisenacher, M., et al. (2019). The PRIDE database and related tools and resources in 2019: improving support for quantification data. Nucleic Acids Res. *47* (*D1*), D442–D450.

Peterson, P.P., and Liu, Z. (2021). Identification and characterization of rapidly accumulating sch9Δ suppressor mutations in Saccharomyces cerevisiae. G3 (Bethesda) *11*, jkab134.

Pinsky, B.A., Kotwaliwale, C.V., Tatsutani, S.Y., Breed, C.A., and Biggins, S. (2006). Glc7/protein phosphatase 1 regulatory subunits can oppose the Ipl1/aurora protein kinase by redistributing Glc7. Mol. Cell. Biol. *26*, 2648–2660.

Plank, M., Perepelkina, M., Müller, M., Vaga, S., Zou, X., Bourgoint, C., Berti, M., Saarbach, J., Haesendonckx, S., Winssinger, N., et al. (2020). Chemical Genetics of AGC-kinases Reveals Shared Targets of Ypk1, Protein Kinase A and Sch9. Mol. Cell. Proteomics *19*, 655–671.

Powis, K., and De Virgilio, C. (2016). Conserved regulators of Rag GTPases orchestrate amino acid-dependent TORC1 signaling. Cell Discov. *2*, 15049.

Quan, Z., Cao, L., Tang, Y., Yan, Y., Oliver, S.G., and Zhang, N. (2015). The yeast GSK-3 homologue Mck1 is a key controller of quiescence entry and chronological lifespan. PLoS Genet. *11*, e1005282.

Reinders, A., Bürckert, N., Boller, T., Wiemken, A., and De Virgilio, C. (1998). *Saccharomyces cerevisiae* cAMP-dependent protein kinase controls entry into stationary phase through the Rim15p protein kinase. Genes Dev. *12*, 2943–2955.

Robinson, J.S., Klionsky, D.J., Banta, L.M., and Emr, S.D. (1988). Protein sorting in *Saccharomyces cerevisiae*: isolation of mutants defective in the delivery and processing of multiple vacuolar hydrolases. Mol. Cell. Biol. *8*, 4936–4948.

Rodríguez-Colman, M.J., Sorolla, M.A., Vall-Llaura, N., Tamarit, J., Ros, J., and Cabiscol, E. (2013). The FOX transcription factor Hcm1 regulates oxidative metabolism in response to early nutrient limitation in yeast. Role of Snf1 and Tor1/Sch9 kinases. Biochim. Biophys. Acta *1833*, 2004–2015.

Salgado, A.P., Schuller, D., Casal, M., Leão, C., Leiper, F.C., Carling, D., Fietto, L.G., Trópia, M.J., Castro, I.M., and Brandão, R.L. (2002). Relationship between protein kinase C and derepression of different enzymes. FEBS Lett. *532*, 324–332.

Sarbassov, D.D., Ali, S.M., and Sabatini, D.M. (2005). Growing roles for the mTOR pathway. Curr. Opin. Cell Biol. *17*, 596–603.

Schmelzle, T., Beck, T., Martin, D.E., and Hall, M.N. (2004). Activation of the RAS/cyclic AMP pathway suppresses a TOR deficiency in yeast. Mol. Cell. Biol. *24*, 338–351.

Schmidt, A., Beck, T., Koller, A., Kunz, J., and Hall, M.N. (1998). The TOR nutrient signalling pathway phosphorylates NPR1 and inhibits turnover of the tryptophan permease. EMBO J. *17*, 6924–6931.

Shannon, P., Markiel, A., Ozier, O., Baliga, N.S., Wang, J.T., Ramage, D., Amin, N., Schwikowski, B., and Ideker, T. (2003). Cytoscape: a software environment for integrated models of biomolecular interaction networks. Genome Res. *13*, 2498–2504.

Shimobayashi, M., Oppliger, W., Moes, S., Jenö, P., and Hall, M.N. (2013). TORC1-regulated protein kinase Npr1 phosphorylates Orm to stimulate complex sphingolipid synthesis. Mol. Biol. Cell *24*, 870–881.

Sikorski, R.S., and Hieter, P. (1989). A system of shuttle vectors and yeast host strains designed for efficient manipulation of DNA in *Saccharomyces cerevisiae*. Genetics *122*, 19–27.

Soppa, U., and Becker, W. (2015). DYRK protein kinases. Curr. Biol. *25*, R488–R489.

Soulard, A., Cremonesi, A., Moes, S., Schütz, F., Jenö, P., and Hall, M.N. (2010). The rapamycin-sensitive phosphoproteome reveals that TOR controls protein kinase A toward some but not all substrates. Mol. Biol. Cell *21*, 3475–3486.

Sutherland, C. (2011). What Are the bona fide GSK3 Substrates? Int. J. Alzheimers Dis. *2011*, 505607.

Talarek, N., Cameroni, E., Jaquenoud, M., Luo, X., Bontron, S., Lippman, S., Devgan, G., Snyder, M., Broach, J.R., and De Virgilio, C. (2010). Initiation of the TORC1-regulated G_0 program requires Igo1/2, which license specific mRNAs to evade degradation via the 5¢-3¢ mRNA decay pathway. Mol. Cell *38*, 345–355.

Tanigawa, M., and Maeda, T. (2017). An *in vitro* TORC1 kinase assay that recapitulates the Gtr-independent glutamine-responsive TORC1 activation mechanism on yeast vacuoles. Mol. Cell. Biol. *37*, e00075-17.

Teng, X., Yau, E., Sing, C., and Hardwick, J.M. (2018). Whi2 signals low leucine availability to halt yeast growth and cell death. FEMS Yeast Res. *18*, foy095.

Torggler, R., Papinski, D., Brach, T., Bas, L., Schuschnig, M., Pfaffenwimmer, T., Rohringer, S., Matzhold, T., Schweida, D., Brezovich, A., and Kraft, C. (2016). Two Independent Pathways within Selective Autophagy Converge to Activate Atg1 Kinase at the Vacuole. Mol. Cell *64*, 221–235.

Torres, J., Di Como, C.J., Herrero, E., and De La Torre-Ruiz, M.A. (2002). Regulation of the cell integrity pathway by rapamycin-sensitive TOR function in budding yeast. J. Biol. Chem. *277*, 43495–43504.

Touati, S.A., Hofbauer, L., Jones, A.W., Snijders, A.P., Kelly, G., and Uhlmann, F. (2019). Cdc14 and PP2A phosphatases cooperate to shape phosphoproteome dynamics during mitotic exit. Cell Rep. *29*, 2105–2119.e4.

Tyanova, S., Temu, T., Sinitcyn, P., Carlson, A., Hein, M.Y., Geiger, T., Mann, M., and Cox, J. (2016). The Perseus computational platform for comprehensive analysis of (prote)omics data. Nat. Methods *13*, 731–740.

Übersax, J.A., and Ferrell, J.E., Jr. (2007). Mechanisms of specificity in protein phosphorylation. Nat. Rev. Mol. Cell Biol. *8*, 530–541.

Umekawa, M., and Klionsky, D.J. (2012). Ksp1 kinase regulates autophagy via the target of rapamycin complex 1 (TORC1) pathway. J. Biol. Chem. *287*, 16300–16310.

Urban, J., Soulard, A., Huber, A., Lippman, S., Mukhopadhyay, D., Deloche, O., Wanke, V., Anrather, D., Ammerer, G., Riezman, H., et al. (2007). Sch9 is a major target of TORC1 in *Saccharomyces cerevisiae*. Mol. Cell *26*, 663–674.

Varlakhanova, N.V., Tornabene, B.A., and Ford, M.G.J. (2018). Feedback regulation of TORC1 by its downstream effectors Npr1 and Par32. Mol. Biol. Cell *29*, 2751–2765.

Wanke, V., Pedruzzi, I., Cameroni, E., Dubouloz, F., and De Virgilio, C. (2005). Regulation of G_0 entry by the Pho80-Pho85 cyclin-CDK complex. EMBO J. *24*, 4271–4278.

Wanke, V., Cameroni, E., Uotila, A., Piccolis, M., Urban, J., Loewith, R., and De Virgilio, C. (2008). Caffeine extends yeast lifespan by targeting TORC1. Mol. Microbiol. *69*, 277–285.

Yabuki, Y., Ikeda, A., Araki, M., Kajiwara, K., Mizuta, K., and Funato, K. (2019). Sphingolipid/Pkh1/2-TORC1/Sch9 signaling regulates ribosome biogenesis in tunicamycin-induced stress response in yeast. Genetics *212*, 175–186.

Yerlikaya, S., Meusburger, M., Kumari, R., Huber, A., Anrather, D., Costanzo, M., Boone, C., Ammerer, G., Baranov, P.V., and Loewith, R. (2016). TORC1 and TORC2 work together to regulate ribosomal protein S6 phosphorylation in *Saccharomyces cerevisiae*. Mol. Biol. Cell *27*, 397–409.

Zaragoza, D., Ghavidel, A., Heitman, J., and Schultz, M.C. (1998). Rapamycin induces the G_0 program of transcriptional repression in yeast by interfering with the TOR signaling pathway. Mol. Cell. Biol. *18*, 4463–4470.

Zhang, H.H., Lipovsky, A.I., Dibble, C.C., Sahin, M., and Manning, B.D. (2006). S6K1 regulates GSK3 under conditions of mTOR-dependent feedback inhibition of Akt. Mol. Cell *24*, 185–197.

Zhang, N., Quan, Z., Rash, B., and Oliver, S.G. (2013). Synergistic effects of TOR and proteasome pathways on the yeast transcriptome and cell growth. Open Biol. *3*, 120137.

STAR★METHODS

KEY RESOURCES TABLE

REAGENT or RESOURCE	SOURCE	IDENTIFIER
Antibodies		
Rabbit anti-pSer^{425}-Gis1 (1:5,000)	De Virgilio lab	N/A
Mouse anti-c-Myc (9E10) (1:3,000)	Santa Cruz Biotechnology	sc-40
Mouse anti-HA (12CA5) (1:1,000)	De Virgilio lab	N/A
Goat anti-mouse IgG-HRP conjugate (1:3,000)	BIO-RAD	1706516
Goat anti-rabbit IgG-HRP conjugate (1:3,000)	BIO-RAD	1706515
Rabbit anti-Adh1 (1:100,000)	Calbiochem	126745
Bacterial strains		
E. coli Rosetta (DE3)	Novagen	70954
E. coli DH5α	CGSC	12384
Chemicals, peptides, and recombinant proteins		
2-nitrophenyl-β-D-galactopyranoside	Sigma-Aldrich	73660
Arg10	Sigma-Aldrich	608033
Arg6	Sigma-Aldrich	643440
C18 Cartridges	Macherey-Nagel	731802
Complete EDTA-free Protease Inhibitor Cocktail	Roche	11-697-498-001
Diabur-Test 5000	Accu-Chek	10647659074
Glutathione Sepharose 4B	GE Healthcare	17-0756-01
HR-X Column	Macherey-Nagel	730936P45
Lys4	Sigma-Aldrich	616192
Lys8	Sigma-Aldrich	608041
Lys-C	FUJIFILM Wako Pure Chemical Corporation	129-02541
Ni-NTA agarose	QIAGEN	30210
Pefabloc	Sigma-Aldrich	76307
PhosSTOP	Roche	04-906-837-001
Phos-tag Acrylamide AAL-107	Wako Chemicals	304-93521
Rapamycin	LC Laboratories	R-5000
ReproSil-Pur 120 C18-AQ, 1.9 μm	Dr. Maisch	r119.aq.
TiO_2	GL Sciences	5020-75010
Trypsin	Promega	V5113
Yeast nitrogen base	CONDA	1553-00
Critical commercial assays		
QuikChange Multi Site-Directed Mutagenesis Kit	Agilent	200514
ECL Western Blotting Detection	GE Healthcare	RPN2106
Deposited data		
MS-RAW files	ProteomeXchange	PXD028028
Original Data	Mendeley Data	https://dx.doi.org/10.17632/wjpppv72v9.2

(*Continued on next page*)

Continued

REAGENT or RESOURCE	SOURCE	IDENTIFIER
Experimental models: Organisms/strains		
BY4741	Euroscarf	[BY4741] *MATa; his3Δ1 leu2Δ0 met15Δ0 ura3Δ0*
BY4742	Euroscarf	[BY4742] *MATα; his3Δ1 leu2Δ0 lys2Δ0 ura3Δ0*
YL515 (Figures 4B, 4C, and S2)	Binda et al., 2009	[BY4741/2] *MATα; his3Δ1 leu2Δ0 ura3Δ0*
YL516	Binda et al., 2009	[BY4741/2] *MATa; his3Δ1 leu2Δ0 ura3Δ0*
YDR096W (Figure 4C)	Euroscarf	[BY4741] *gis1Δ::kanMX4*
LD6121 (Figure 4C)	This study	[YL515] $gis1^{S398A,S399A,S400A,S421A,S424A,S425A}$
MP150 (Figures 4B and 4C)	This study	[BY4742] *yak1Δ::kanMX4*
LD6032 (Figures 4B and 4C)	This study	[BY4742] *cdc55Δ::hisMX6 yak1Δ::kanMX4*
YSB148 (Figures 4B and 4C)	Bontron et al., 2013	[BY4741] *cdc55Δ::kanMX6*
CDV288-12B (Figures 4B and 4C)	This study	[BY4742] *igo1Δ::kanMX4 igo2Δ::kanMX2*
YFL033C (Figures 4B and 4C)	Euroscarf	[BY4741] *rim15Δ::kanMX4*
YSB150 (Figures 4B and 4C)	Bontron et al., 2013	[YL516] *cdc55Δ::kanMX6 rim15Δ::natMX4*
LD6181 (Figure 4C)	This study	[BY4741] *cdc55Δ::hphNT1 gis1Δ::kanMX4*
LD6182 (Figure 4C)	This study	[YL515] *cdc55Δ::hphNT1* $gis1^{S398A,S399A,S400A,S421A,S424A,S425A}$
MJ5682 (Figures 3, S1, and S3; Tables S1 and S2)	Hu et al., 2019	[YL515] *arg4Δ::hisMX4 lys2Δ::hphNT1*
LD5320 (Figures 3, S1, and S3; Tables S1 and S2)	This study	[YL516] *rim15Δ::hphNT1 arg4Δ::URA3 lys2Δ0*
LD5321 (Figures 3, S1, and S3; Tables S1 and S2)	This study	[YL516] *yak1Δ::hphNT1 arg4Δ::URA3 lys2Δ0*
LD5757 (Figures 3, S1, and S3; Tables S1 and S2)	This study	[YL515] *npr1Δ::natNT2 arg4Δ::hisMX4 lys2Δ::hphNT1*
LD5758 (Figures 3, S1, and S3; Tables S1 and S2)	This study	[YL515] *slt2Δ::natNT2 arg4Δ::hisMX4 lys2Δ::hphNT1*
SEY6210	Robinson et al., 1988	*MATα; leu2-3,112 ura3-52 his3-Δ200 trp1-Δ901 suc2-Δ9 lys2-801; GAL*
YKF001 (Figures 5A–5C)	Feng et al., 2016	[SEY6210] *atg9Δ::LEU2 ATG9-GFP::URA3 pho13Δ pho8Δ60*
YKF002 (Figures 5A–5C)	Feng et al., 2016	[SEY6210] *atg9Δ::LEU2* $atg9^{S122A}$*-GFP::URA3 pho13Δ pho8Δ60*
YKF003 (Figures 5A–5C)	Feng et al., 2016	[SEY6210] *atg9Δ::LEU2* $atg9^{S122D}$*-GFP::URA3 pho13Δ pho8Δ60*
LD6175 (Figures 5A–5C)	This study	[SEY6210] *npr1Δ::hphNT1 atg9Δ::LEU2 ATG9-GFP::URA3 pho13Δ pho8Δ60*
LD6176 (Figures 5A–5C)	This study	[SEY6210] *npr1Δ::hphNT1 atg9Δ::LEU2* $ATG9^{S122D}$*-GFP::URA3 pho13Δ pho8Δ60*
YMM31-1A (Figure S2)	This study	[YL515] *slt2Δ::kanMX4*
LD6069 (Figure 5D)	This study	[YL515] *npr1Δ::hphNT1*
Recombinant DNA		
pLD3533 (Figure 4A)	This study	[pET-24d] *YAK1-HA*
pLD3896 (Figure 4A)	This study	[pET-Duet] *GIS1-*myc_{13}
pLD3930 (Figure 4A)	This study	[pET-Duet] $gis1^{S425A}$-myc_{13}
pSB009 (Figure 4B)	Bontron et al., 2013	CEN/ARS, *URA3, ADH1p-GIS1-*HA_3
pSB010 (Figure 4B)	Bontron et al., 2013	CEN/ARS, *URA3, ADH1p-*$gis1^{S425A}$-HA_3
pLD3707 (Figures 4B and 4C)	This study	CEN/ARS, *MET15*
pRS317 (Figures 4B and 4C)	Sikorski and Hieter, 1989	CEN/ARS, *LYS2*
pLD3920 (Figure 4C)	This study	CEN/ARS, *URA3, SSA3-lacZ*

(*Continued on next page*)

Continued

REAGENT or RESOURCE	SOURCE	IDENTIFIER
pDP245 (Figures 5A and 5B)	Torggler et al., 2016	CEN/ARS, *HIS3, APE1p-TagBFP-APE1, CUP1p-APE1*
pLD4150 (Figure S2)	This study	CEN/ARS, *LEU2, SLT2*
pRS415 (Figure S2)	Brachmann et al., 1998	CEN/ARS, *LEU2*
pAS103 (Figure S2)	Schmidt et al., 1998	2μ, *URA3, HA-NPR1*
pBS2 (Figure 5D)	Bonenfant et al., 2003	2μ, *URA3, GST-NPR1*
pBS3 (Figure 5D)	Bonenfant et al., 2003	2μ, *URA3, GST-npr1^{K467R}*
pLD4159 (Figur 5D)	This study	[pET15b] *ATG9$^{1-315}$*
Software and algorithms		
ClueGO 2.5	Bindea et al., 2009	http://apps.cytoscape.org/apps/cluego
Cytoscape 3.8.2	Shannon et al., 2003	https://cytoscape.org
ImageJ	NIH	https://imagej.nih.gov/ij/index.html
MaxQuant	Cox and Mann, 2008	https://maxquant.net/maxquant/
MV_pairwise_alignment	N/A	https://github.com/mvisani/MV_pairwise_alignment
Perseus	Tyanova et al., 2016	https://maxquant.net/perseus/
Prism 8	Graphpad	https://www.graphpad.com/scientific-software/prism/
WebLogo 3	Crooks et al., 2004	https://weblogo.berkeley.edu

RESOURCE AVAILABILITY

Lead contact

Further information and requests for resources and reagents should be directed to and will be fulfilled by the Lead Contact, Claudio De Virgilio (claudio.devirgilio@unifr.ch).

Materials availability

All unique/stable reagents generated in this study are available from the Lead Contact.

Data and code availability

- The mass spectrometry proteomics data have been deposited to the ProteomeXchange Consortium via the PRIDE partner repository with the dataset identifier PRIDE Archive: PXD028028 (Perez-Riverol et al., 2019). Source data for gel images and graphs can be found in Mendeley Data: https://dx.doi.org/10.17632/wjpppv72v9.2
- This paper does not report original code.
- Any additional information required to reanalyze the data reported in this paper is available from the Lead Contact upon request.

EXPERIMENTAL MODEL AND SUBJECT DETAILS

Saccharomyces cerevisiae strains used in this study are listed in the key resources table. They were grown as described in method details below. Recombinant proteins were expressed in *Escherichia coli* Rosetta (DE3) and cloning procedures were carried out in *E. coli* DH5α.

METHOD DETAILS

Yeast strains, plasmids, and growth conditions

Saccharomyces cerevisiae strains and plasmids are listed in key resources table. CRISPR-Cas9 genome editing was performed as described (Generoso et al., 2016). Gene deletion was performed using the pFA6a system-based PCR-toolbox (Janke et al., 2004). Plasmid mutagenesis was performed using the QuikChange Multi Site-Directed Mutagenesis Kit (Agilent). Unless otherwise stated, yeast strains were grown to mid-log phase in synthetic dextrose (SD) medium (0.17% yeast nitrogen base, 0.5% ammonium sulfate, and 2% glucose) at 30°C. For *in vivo* SILAC experiments, yeast strains were grown in synthetic dextrose complete medium containing either non-labeled or labeled lysine (30 mg L^{-1}) and arginine (30 mg L^{-1}) variants: ''Heavy'' L-arginine-$^{13}C_6$-$^{15}N_4$ (Arg10) and L-lysine-$^{13}C_6$-$^{15}N_2$

(Lys8), or ''medium'' L-arginine-$^{13}C_6$ (Arg6) and L-lysine-$^{2}H_4$ (Lys4) amino acids (Sigma-Aldrich) were used as labels. Cells were treated or not with 200 ng mL^{-1} rapamycin for 30 min. The following double and triple labeling experiments were performed (three biological replicates each, 18 SILAC analyses in total):

Light label	Medium label	Heavy label
WT + Rapamycin	*rim15*Δ + Rapamycin	*yak1*Δ + Rapamycin
WT + Rapamycin	*slt2*Δ + Rapamycin	*npr1*Δ + Rapamycin
*npr1*Δ - Rapamycin	-	*npr1*Δ + Rapamycin
*yak1*Δ - Rapamycin	-	*yak1*Δ + Rapamycin
*slt2*Δ - Rapamycin	*slt2*Δ + Rapamycin	-
*rim15*Δ - Rapamycin	*rim15*Δ + Rapamycin	-

Data comparison was performed by using respective common samples for normalization.

MS sample preparation, phosphopeptide enrichment, and LC-MS/MS and data analyses

MS samples and LC-MS/MS analyses were performed as described in Dokládal et al. (2021) and Hu et al. (2019). Briefly, yeast strains were grown in synthetic dextrose complete medium containing either non-labeled or labeled lysine and arginine variants. Dried TCA-treated cell pellets (100 mg) of each label were mixed, proteins extracted with 8 M urea, reduced and alkylated with DTT (1 mM) and iodoacetamide (5 mM), respectively, and digested by Lys-C (WAKO) for 4 h at RT. Urea was diluted to 1 M and trypsin (Promega) digestion was performed overnight. The next day, peptides were purified by SPE (HR-X columns and C18 cartridges; Macherey-Nagel), eluates were frozen in liquid nitrogen and lyophilized overnight. The next day, peptides were fractionated by HpH RP-chromatography, fractions were acidified, frozen in liquid nitrogen, and lyophilized overnight. The fourth day, dried peptides were suspended in 200 μl 80% acetonitrile/1% TFA for phosphopeptide enrichment. Phosphopeptides were enriched by TiO_2 beads (GL Sciences). The tip flow-through was used for non-phosphopeptide analysis. LC-MS/MS measurements were performed on a QExactive (QE) Plus (peptides) and HF-X (phosphopeptides) mass spectrometer coupled to an EasyLC 1000 and EasyLC 1200 nanoflow-HPLC, respectively (all Thermo Scientific). Peptides were separated on a fused silica HPLC-column tip (I.D. 75 μm, New Objective, self-packed with ReproSil-Pur 120 C18-AQ, 1.9 μm [Dr. Maisch] to a length of 20 cm) using a gradient of A (0.1% formic acid in water) and B (0.1% formic acid in 80% acetonitrile in water). Mass spectrometers were operated in the data-dependent mode; after each MS scan (mass range m/z = 370 – 1750; resolution: 70,000 for QE Plus and 120,000 for HF-X) a maximum of ten, or twelve MS/MS scans were performed using a normalized collision energy of 25%, a target value of 1,000 (QE Plus) or 5,000 (HF-X), and a resolution of 17,500 for QE Plus and 30,000 for HF-X. MS raw files were analyzed using MaxQuant (version 1.6.2.10) (Cox and Mann, 2008) using a UniProt full-length *S. cerevisiae* database (March, 2016) and common contaminants, such as keratins and enzymes used for in-gel digestion, as reference. Carbamidomethylcysteine was set as fixed modification and protein amino-terminal acetylation, serine-, threonine- and tyrosine- phosphorylation, and oxidation of methionine were set as variable modifications. MS/MS tolerance was 20 ppm and three missed cleavages were allowed using trypsin/P as enzyme specificity. Peptide, site, and protein FDR based on a forward-reverse database were set to 0.01, minimum peptide length was set to 7, the minimum score for modified peptides was 40, and minimum number of peptides for identification of proteins was set to one, which must be unique. MaxQuant results were analyzed using Perseus (Tyanova et al., 2016).

GO-term analyses were performed with Cytoscape 3.8.2 (Shannon et al., 2003) and ClueGO 2.5.3. (Bindea et al., 2009). The GO cellular compartment enrichment was calculated compared to the yeast genome and GO term fusion was used. Only pathways with a p value ≤ 0.05 were determined as significant (Bonferroni step-down corrected). The GO tree interval was set between 3 and 8. GO clusters contained at least 5 genes or 4% of genes.

Protein purification and Npr1 *in vitro* kinase assay

GST-Npr1 and GST-Npr1^{K467R} were expressed in an *npr1*Δ strain. The cells were grown in synthetic raffinose medium (0.17% yeast nitrogen base, 0.5% ammonium sulfate, 2% raffinose, and 0.1% sucrose) lacking uracil. At OD_{600} of 0.5, galactose (2%) was added, the cells were further grown for 4 h and treated for 30 min with 200 ng mL^{-1} rapamycin before being collected by filtration and frozen in liquid nitrogen. Cells were then disrupted with glass beads (0.25-0.50 mm diameter; Retsch) in lysis buffer (phosphate-buffered saline [pH 7.3], 1 × cOmplete EDTA free protease inhibitor cocktail (Roche), 1 × Pefabloc SC (Sigma), 1 × PhosSTOP (Roche), and 0.5% Nonidet P40) using a Fast-Prep-24TM (MP Biomedicals; 5,000 rpm, 6 × 30 s, 1 min pause). The lysates were clarified by centrifugation (3,220 × *g*, 5 min, 4°C) and incubated at 4°C for 2 h with glutathione Sepharose 4B (GE Healthcare). The resin was then washed three times with phosphate-buffered saline (pH 7.3) and bound GST-Npr1 variants were eluted with 50 mM Tris-HCl (pH 8.0), 10 mM glutathione, and 10% glycerol, for 30 min at room temperature.

Recombinant His_6-$Atg9^{1-315}$ was purified from *E. coli* Rosetta (DE3). The bacteria were lysed in 50 mM sodium phosphate (pH 8), 300 mM NaCl, 10 mM imidazole, 1 × cOmplete EDTA free protease inhibitor cocktail (Roche), 1 × Pefabloc SC (Sigma), 1 × PhosSTOP

(Roche), 1 mM DTT, and 0.1% Nonidet P40, and the clarified lysates were incubated at 4°C for 2 h with Ni-NTA agarose (QIAGEN). The resin was then washed three times with 50 mM sodium phosphate (pH 8.0), 300 mM NaCl, and 50 mM imidazole and bound His_6-$Atg9^{1-315}$ was eluted with 50 mM sodium phosphate (pH 8), 300 mM NaCl, 250 mM imidazole, and 10% glycerol, for 1 h at 4°C. For Npr1 *in vitro* kinase assay, 40 μL of purified GST-Npr1 or GST-$Npr1^{K467R}$ were mixed with 40 μL of His_6-$Atg9^{1-315}$ purified from *E. coli*, in kinase assay buffer (50 mM Tris-HCl [pH 7.5], 2 mM $MnCl_2$). The reaction (400 μL) was started by addition of 1 mM ATP, the samples were incubated for 30 min at 37°C, and analyzed by MS as described (Hu et al., 2019).

Cell lysate preparation and immunoblot analysis

Yeast cells were treated with 6.3% w/v trichloroacetic acid (final concentration) for at least 10 min on ice, pelleted, washed with ice-cold acetone, dried, disrupted with glass beads in urea buffer (50 mM Tris.Cl [pH 7.5]), 6 M urea, 1% SDS, 1 × Pefabloc SC (Sigma), and 50 mM NaF) using a Precellys homogenizer, and boiled for 5 min in 2-mercaptoethanol containing Laemmli sample buffer. *E. coli* lysates were prepared by boiling bacterial pellets for 10 min in Laemmli sample buffer and centrifuging for 10 min at 16,000 × *g*. Gis1-Ser^{425} phosphorylation was monitored using a rabbit polyclonal phosphospecific anti-$pSer^{425}$-Gis1 antibody (dilution 1:5,000; GenScript). For HA-tag and c-Myc-tag detection, mouse anti-HA 12CA5 (dilution 1:1,000) or anti-c-Myc 9E10 (dilution 1:3,000; Santa Cruz Biotechnology) antibodies were used, respectively. HA-Npr1 phosphorylation was assessed by phosphate-affinity gel electrophoresis on 6% SDS-PAGE gels containing 25 μM Phos-tag (Wako) and 50 μM $MnCl_2$. ECL Western Blotting Detection (GE Healthcare) was used for the western blot development.

β-galactosidase assays

To test the *SSA3-LacZ* activity, cells were grown in SD medium lacking uracil for 48 h. Glucose deprivation was checked using Diabur-Test 5000 (Accu-Chek). Cell pellets were resuspended in Z-buffer and processed for β-galactosidase assay with the SDS/chloroform cell permeabilization method as previously described (Guarente, 1983). β-galactosidase activity was measured using 2-nitrophenyl-β-D-galactopyranoside (Sigma-Aldrich) as substrate.

Fluorescence microscopy

To monitor the Atg9-GFP colocalization with BFP-Ape1, cells were grown in SD medium lacking histidine and then starved for nitrogen for 30 min. Images of live fluorescent cells were captured with an inverted spinning disk confocal microscope Visitron VisiScope CSU-W1 that was equipped with a scientific grade 4.2 sCMOS camera and a 100 × 1.3 NA oil immersion Nikon CFI series objective, and processed using ImageJ software. For each strain, at least 80 cells were recorded and the pictures show representative cells in each case.

ALP assays

Autophagy was induced by shifting the cells for 4 h to nitrogen starvation medium according to (Noda et al., 1995). Autophagic flux was determined as described (Klionsky et al., 2021).

QUANTIFICATION AND STATISTICAL ANALYSIS

To identify rapamycin sensitive, potential kinase target sites by MS-based proteomics, we combined the measurement of the log2-fold change on each site and for 17 replicates per kinase (5x wt+/wt-, 5x wt+/*atg1*Δ-, 4x wt+/Kol delta-, 3x wt+/Kol delta+) into a random effect model as described, yielding an average effect size and its corresponding 95% confidence interval for each site (Dokládal et al., 2021; Hu et al., 2019). Sites had to be (i) significant according to the random effect model and (ii) minimally 2-fold regulated in (a) cells treated or not with rapamycin, and (b) comparing WT and Kol delta cells both treated with rapamycin (log2 $\geq$ 0.95). Sites regulated comparing Kol delta cells treated or not with rapamycin were excluded (negative control).

If not otherwise stated, three independent biological replicates were performed and analyzed for statistically significant differences using unpaired Student's t tests employing the following annotation: *p $\leq$ 0.05; **p $\leq$ 0.001; ***p $\leq$ 0.0001.